ADVANCES IN FATIGUE AND FRACTURE MECHANICS ANALYSES FOR AIRCRAFT STRUCTURES

J. C. Newman, Jr.*

This paper reviews some of the advances that have been made in stress analyses of cracked aircraft components, in the understanding of the fatigue and fatigue-crack growth process, and in the prediction of residual strength of complex aircraft structures with widespread fatigue damage. Finite-element analyses of cracked structures are now used to determine accurate stress-intensity factors for cracks at structural details. Observations of small-crack behavior at open and rivet-loaded holes and the development of small-crack theory has lead to the prediction of stress-life behavior for components with stress concentrations under aircraft spectrum loading. Fatigue-crack growth under simulated aircraft spectra can now be predicted with the crack-closure concept. Residual strength of cracked panels with severe out-of-plane deformations (buckling) in the presence of stiffeners and multiple-site damage can be predicted with advanced elastic-plastic finite-element analyses and the critical crack-tip-opening angle (CTOA) fracture criterion. These advances are helping to assure continued safety of aircraft structures.

INTRODUCTION

In 1969, Schijve in the Second Frederik J. Plantema Memorial Lecture [1] stated that "fatigue in aircraft structures is a problem for which quantitative and generally accepted solutions are not available." During the past 30 years, many advances have been made in the stress analyses of cracked aircraft components, in understanding the fatigue and fatigue-crack growth behavior in metallic materials, and in the prediction of residual strength of complex built-up aircraft structures with widespread fatigue damage. Although the failure rate in aircraft structures due to fatigue and structural failure has dropped significantly [2] from the mid-1950's, the fatigue and fracture community must stay alert. The technical community should continue to improve the understanding of the fatigue and fracture process and to use the advanced analysis tools to safe guard the public against unexpected failure modes, such as the Aloha Airlines fuselage failure in 1988 due to widespread fatigue damage. Swift, in the Eleventh Plantema Lecture [3], discussed how multiple-site damage cracking could reduce the residual strength of fuselage structures.

The Seventeenth Plantema Memorial Lecture is a review of some of the technical developments and concepts that have led to a better understanding of the fatigue and fracture process in metallic materials. Advances in computer technology has allowed more accurate stress analyses to be conducted on three-dimensional crack configurations, more realistic simulations of fatigue and fatigue cracking in structural components, and the use of more advanced elastic-plastic fracture

* Mechanics and Durability Branch, NASA Langley Research Center, Hampton, VA, USA 23681

mechanics concepts to assess the residual strength and fail-safe capability of aircraft structures. This review is limited in scope and will not be able to fully cover the vast amount of research that has been conducted over the past 30 years in the fields of fatigue and fracture mechanics. The author requests the readers indulgence and forgiveness if some major events have been omitted, or if reference is not made to all of those who have made significant contributions to the subject.

In particular, this paper will review some of the advances that have been made in the area of stress analyses of cracked bodies, fatigue (crack-initiation and small-crack behavior), fatigue-crack growth, and fracture of complex fuselage structure. The paper will discuss the global stress analyses of cracked fuselage lap-joint structure to determine local fastener stresses. These local stresses are then used to develop stress-intensity factors for surface and corner cracks at open and fastener-loaded holes using three-dimensional codes. Observations of small-crack behavior at open and rivet-loaded holes and the development of small-crack theory have lead to the prediction of stress-life behavior for components under constant- and variable-amplitude loading. Some of these predictions are shown for materials commonly used in aircraft construction. Fatigue crack growth under aircraft spectrum loading can be predicted with the crack-closure concept. The importance of constraint (three-dimensional stress state around the crack front) on fatigue-crack growth under spectrum loading will be discussed. The ability of the advanced finite-element codes to predict the severe out-of-plane deformations of cracked sheets is demonstrated. Predictions of residual strength of cracked panels with severe out-of-plane deformations in the presence of stiffeners and multiple-site damage cracking will be demonstrated with advanced finite-element codes and the critical crack-tip-opening angle (CTOA) fracture criterion. In the last decade, the international conferences on aging aircraft [4-6] have intensified the development of these advanced methodologies and tools for fatigue and fracture mechanics analyses, see for example Harris et al [7]. These advances are helping to insure the continued airworthiness of aircraft structures.

STRESS ANALYSES OF CRACKED BODIES

During the past 30 years, the stress-analysis community has developed a large number of finite-element codes to conduct linear and non-linear stress analyses of complex aircraft structural components. Many aircraft companies determine stress and deformation states in aircraft structures using codes, such as ABAQUS [8], ANSYS [9], MSC/NASTRAN [10] and STAGS [11,12]. Many of these codes have special features to analyze crack problems and determine the stress-intensity factor or the non-linear equivalent, the J-integral. Some of these codes, such as ABAQUS and STAGS, have incorporated the critical crack-tip-opening angle (or displacement) fracture criterion for conducting material and geometric non-linear fracture analyses of complex structures. The developers of STAGS have also incorporated the “plane-strain” shell element [12] for more accurate fracture simulations of cracked shell structure.

At NASA Langley, some specialty codes have been developed to conduct fatigue and fracture mechanics analyses of cracked specimens and structural components. These codes were developed to calculate crack-tip parameters or to study new fatigue and fracture criteria. The ZIP2D code [13] was one of the firsts to be used for fatigue-crack growth simulations to study the crack-closure mechanism. This code was also used to study the critical crack-tip-opening

displacement (CTOD) fracture criterion. Later, SURF3D [14] and ZIP3D [15] were developed to calculate stress-intensity factors for surface and corner cracks in plates or at holes. The ZIP3D code also incorporated material non-linear (small strain) effects to study the J-integral and three-dimensional fatigue-crack growth and closure.

A number of the universities and companies involved in the NASA Airframe Structural Integrity Program [7] have also developed codes to conduct stress and deformation analyses of cracked specimens and structural components. Chang and Mear [16] developed the FADD2D code to determine mixed-mode stress-intensity factors for almost any two-dimensional crack configuration subjected to either stress or displacement boundary conditions. The FADD2D code is based on a boundary-element method with some special dislocation formulations to model arbitrarily shaped cracks. Ingraffea and his colleagues [17,18] have developed a series of codes, FRANC2D and FRANC3D, to conduct linear and non-linear stress analyses of two- and three-dimensional bodies with arbitrarily shaped cracks. The FRANC2D code is based on a finite-element approach, whereas the FRANC3D code is based on the boundary-element formulation. Dodds and his students [19] have also developed an advanced material and geometric non-linear code, WARP3D, based on the three-dimensional finite-element method. This code has some special features to study fracture simulations using either a void-growth model or the critical CTOA. Later, some results from these codes will be presented to demonstrate their capabilities.

In the NASA aging aircraft program, a unique capability has been developed that integrates the fracture topology modeling capabilities of FRANC3D with the general shell analysis capabilities of STAGS into an integrated FRANC3D/STAGS analysis procedure [18]. The automatic adaptive remeshing capability of FRANC3D and the geometric non-linear stress-analysis capability of STAGS provide the analysis basis required to predict the crack growth, crack turning, and crack arrest behavior exhibited by pressurized shell structures in damage-tolerant tests. The integrated FRANC3D/STAGS analysis procedure currently operates on high-level workstations or on mainframe computers. This capability is described in greater detail in References 7 and 18.

Analysis Methodology for Riveted Lap Joints

The general strategy for developing the structural analysis methodology for predicting the stress and deformation states in stiffened shells is shown in Figure 1. Large-scale global models of a stiffened fuselage shell of interest are developed and analyses are conducted to determine the internal stress distributions and general response of the shell. A hierarchical modeling approach is used to provide highly refined local models, which are developed based on the global model results. The local model provides the higher fidelity solutions that are necessary to calculate the local stresses and rivet loading in the lap-joint region. To determine accurate rivet-load transfer, the rivet is modeled with rigid links (stiff springs) and sheets are connected by a rivet spring with 6 degrees of freedom (3 translational and 3 rotational). Examples of these analysis capabilities are demonstrated in References 20 and 21.

Over the last 30 years, several laboratories have tested lap-joint specimens to determine the influence of manufacturing processes and environment on fatigue life. An extensive test program

was conducted by Hartman [22], at the National Aerospace Laboratory (NLR), to assess the effects of many manufacturing variables on the fatigue behavior of thin-sheet riveted lap joints, as shown in Figure 2(a). Manufacturing variables such as the joint configuration, type of fastener, surface treatment of the metal prior to riveting, and several different riveting techniques were investigated. All specimens had straight-shank button-head rivets and were tested under ambient conditions with constant-amplitude tension-tension fatigue loading or a variable-amplitude block-program loading. Further details of the test program and an analysis of the test results are given by Newman et al [23]. Later, Furuta et al [24], at the Kawasaki Heavy Industries (KHI) and the National Aerospace Laboratory (NAL), tested similar lap-joint specimens with two- or three-rivet rows using 100 degree countersunk rivets. These tests were conducted under either ambient conditions or immersed in a 3.5 % salt-water solution. An analysis of these test data is given by Harris et al [25]. Herein, the test and analysis results under ambient conditions will also be presented to demonstrate the application of small-crack theory to lap-joint specimens. Fatigue testing on a full-scale aircraft indicated that after about 66,000 pressure cycles extensive cracking had developed at a lap joint [26] with 4-rivet rows, like that shown in Figure 2(b). An analysis of these data [27] indicated that the riveted joint might be considered as a "neat-fit" joint with very little rivet-hole interference and minimal clamp-up effects. A crack-growth analysis using only the rivet load, by-pass stress, and local bending stress was sufficient to match the crack-growth rates measured from the fuselage panel.

The fatigue analyses of the riveted lap-joint specimens, presented in References 23 and 25, were based on stress-intensity factors for through cracks and corner cracks at a rivet-loaded hole, as shown in Figure 3. From the global-local finite-element stress analyses (Fig.1), the rivet loading (P), by-pass stress (S_b), and local bending moment (M) were determined. The rivet interference (Δ) and stresses due to local clamp-up effects are unknown parameters that are very difficult to determine. Thus, an "effective" interference level was used to estimate interference and clamp-up effects in the NLR specimens [23]. But for the KHI-NAL lap-joint specimens with the 100 degree countersunk rivets, no rivet-hole interference was required to fit the test data [25].

Stress-Intensity Factor Analyses

Two of the codes from the NASA toolbox [7] were used to determine stress-intensity factors for through cracks at a rivet-loaded hole in a lap joint. The FRANC2D/L code (FRANC2D code with layering capability [17]) and the FADD2D code [16] were used to analyze two symmetric cracks emanating from a rivet-loaded hole in a segment from a lap-joint specimen. The insert in Figure 4 shows the configuration analyzed. This configuration models the lap-joint specimen shown in Figure 2(a) with a 50% by-pass load. The FRANC2D/L code was used to analyze the rivet and rivet-hole contact and the stress-intensity factors are shown as circular symbols. In the FADD2D analysis, the rivet was not modeled but the rivet-contact stresses were used to load the hole boundary. The square symbols show the FADD2D results, which agreed well with the FRANC2D/L results. The solid curve is an equation [23] that was fit to these results.

The determination of stress-intensity factors (K) for three-dimensional cracks, such as a surface and corner crack in a plate or at a hole, has greatly improved in the last 20 years. In 1979, Newman [28] reviewed the stress-intensity factors for a surface crack in a plate. A comparison of

the K solutions from the literature for a semi-elliptical surface crack in a plate subjected to remote tension is shown in Figure 5(a). The normalized stress-intensity factor is plotted against the crack-depth-to-plate-thickness (a/t) ratio. The dashed curves are from tabular results and the solid curves are from equations. See Reference 28 for details on the various methods used to obtain these K solutions. This plot demonstrated that the K solution from various researchers varied by almost 100% for the same crack configuration. The dark solid curve is the equation developed by Newman and Raju that was fit to their finite-element results [29]. After twenty years, the Raju-Newman solutions have been shown by other investigators to be within about 5% of the accepted solution.

In 1999, Bakuckas [30] conducted an analytical round robin to assess the capability of stress analysts, using some of the newer advanced codes, to determine the stress-intensity factors for a corner crack emanating from an open hole under remote tension. These results are shown in Figure 5(b). The hole-radius-to-plate-thickness (r/t) ratio was 2 and the hole-radius-to-plate-half-width (r/w) was 0.2. The crack-shape ratio (a/c) was 0.8 and the crack-depth-to-plate-thickness (a/t) ratio was 0.2. Six analysts tried either finite-element (FEM, FEAM), boundary-element (BEM, FADD) or weight-function (WFM) methods to solve the crack problem. The dark solid curve is, again, the Newman-Raju equation (also fit to their finite-element results [31]) for this crack configuration. See Reference 30 for details on the various solutions methods. All of the results were within about 5% of each other. These results demonstrate that three-dimensional stress-analysis codes can now be used to obtain accurate stress-intensity factors at the structural detail level.

Software Validation

One of the objectives in the NASA aging aircraft program [7] was to develop and validate advanced stress analysis codes or validate existing codes for analyzing the stress and deformation states in a cracked fuselage structure. A crack in a pressurized cylinder, like a fuselage, will bulge due to the internal pressure. Because of crack-tip yielding and large out-of-plane deformations, a material and geometric non-linear code was required. Both the STAGS and the WARP3D codes had the potential to predict the out-of-plane deformations. To verify these codes, a large tension panel with a central slot of 102 mm in length (2c) was tested to measure the out-of-plane deformations (see the insert in Fig. 6). The ends of the slot had a drilled circular hole of 2.4 mm in radius. The holes were used to prevent a crack from developing and extending until a very high load was reached. The measured out-of-plane displacements are shown as symbols in Figure 6 at an applied stress of 240 MPa. The displacements were measured along the dashed line shown in the insert at a y/w value of 0.125. The solid curve is the calculations from a WARP3D analysis [32]. The three-dimensional, elastic-plastic, large-deformation analysis agreed well with the test measurements made using a digital-imaging method [33].

In summary, stress-analysis codes and methods are available to determine the stress and deformation states of aircraft structural components with and without cracks. Accurate stress-intensity factors can now be determined for two- and three-dimensional crack configurations for use in durability and damage-tolerance analyses. Material and geometric non-linear analyses

codes can be used to predict the stress and deformation states for complex structure. Some of these codes have been validated by comparing with experimental test data.

FATIGUE OF METALLIC MATERIALS

The fatigue life of a metallic material is divided into several phases: crack nucleation, micro-crack growth, macro-crack growth, and failure. Crack nucleation is associated with cyclic slip and is controlled by the local stress and strain concentrations. Although the slip-band mechanism of crack formation may be necessary in pure metals, the presence of inclusions or voids in engineering metals will greatly affect the crack-nucleation process. Micro-crack growth, a term now referred to as the "small-crack growth" regime, is the growth of cracks from inclusions, voids, or slip bands, in the range of 1 to 20 μm in length. Schijve [34] has shown that for polished surfaces of pure metals and for commercial alloys, the formation of a small crack to about 100-μm in size can consume 60 to 80 % of the fatigue life. The AGARD [35,36] and NASA/CAE [37] studies on small-crack behavior showed that about 90% of the fatigue life were consumed for crack growth from about 10 μm to failure on a variety of materials. This is the reason that there is so much interest in the growth behavior of small cracks. Macro-crack growth and failure are regions where fracture-mechanics parameters have been successful in correlating and in predicting fatigue-crack growth and fracture. This review will highlight the advances that have been made in the use of the same fracture-mechanics parameters in the treatment of micro- or small-crack growth using continuum-mechanics approaches.

Small-Crack Behavior

Aluminum Alloy 7075-T6—Earlier work by Pearson [38] on fatigue-crack initiation and growth of small cracks from inclusion particles in two aluminum alloys (BS L65 and DTD 5050) set the stage for the development of small-crack theory. His results are shown in Figure 7 as the dotted curve, along with additional small-crack data (light solid curves) from Lankford [39] on 7075-T6 aluminum alloy using un-notched ($K_T = 1$) specimens. These tests were conducted at a stress ratio ($R = S_{min}/S_{max}$) of 0.05. Lankford's data went down to ΔK values as low as 1.5 MPa$\sqrt{m}$. They both concluded that cracks of about the average grain size grew several times faster than large cracks at nominally identical ΔK values. The open symbols and dash-dot curve show the large-crack data and the development of the large-crack threshold at about 3 to 4 MPa$\sqrt{m}$. Some general observations from Lankford were that the minimum in dc/dN occurred when the crack length, c, was about the minimum dimension of the grain size and that the magnitude of the lower rates was controlled by the degree of micro-plasticity in the next grain penetrated by the crack. If the next grain is oriented like the first, then no deceleration will occur, as indicated by the uppermost small-crack curves.

At this stage, it would be of interest to compare the test results from Pearson and Lankford with the small-crack growth predictions made from the continuum-mechanics model based on crack closure [40,41]. The baseline ΔK_{eff}-rate relation used in the FASTRAN closure model [42,43] was obtained from Reference 44. The constraint factor (α) used in the analysis was 1.8 for rates

less than 7E-4 mm/cycle. The constraint factor accounts for the effects of stress state on crack-growth rate behavior (plane stress or plane strain) and was used to correlate the large-crack growth rate data for various stress ratios (R). The ΔK_{eff}-rate results were generated from large-crack data for rates greater than about 2E-6 mm/cycle. The lower section of the ΔK_{eff}-rate relation (below 2E-6 mm/cycle) was estimated on the basis of small-crack data [37]. Because small cracks are assumed to be fully open on the first cycle, the ΔK_{eff}-rate relation is the starting point for small-crack analysis. The results of an analysis of the test specimen used by Lankford are shown by the heavy solid curve. The initial defect was selected as a 10-μm radius semi-circular surface crack. As the small crack grew, the closure level increased much faster than the ΔK level and a rapid decrease in rates was calculated. The rapid drop is a combination of the closure transient and the sharp change in slope of the ΔK_{eff}-rate relation (at about 1E-6 mm/cycle). At about 30 μm, the crack-opening stresses had nearly stabilized. The predicted small-crack results are in excellent agreement with Pearson's data and agree with some of Lankford's data, which did not exhibit a grain-boundary influence. But interestingly, the small-crack analysis showed a single dip in the small-crack curve, similar to the "single" dip observed in some of Lankford's small-crack data. Would the grain-boundary interaction always occur at the same crack length (40 μm)? Why aren't there other dips, or small indications of a dip, in the rate curve at 80 or 120 μm? Similarly, a shift in the ΔK_{eff}-rate relation to higher ΔK_{eff} values in the near-threshold regime and a larger initial defect would also shift the analysis "dip" to higher ΔK values, closer to the test data. Further study is needed to help resolve these issues.

The results shown in Figure 7 demonstrate that small-crack data is the "typical" data and that the large-crack data, approaching the large-crack threshold, is the "anomaly." There are no models that can predict the development of the large-crack threshold but the growth of small cracks (30 μm or greater in this alloy) are growing under steady state conditions (constant crack-opening stresses). In the 1980's, it was thought that the small-crack effect was the anomaly and that the large-crack data approaching the threshold was the correct data. During the last decade, research on the large-crack threshold behavior has demonstrated that the threshold is being caused by a rise in crack-closure behavior (due to plasticity-, roughness-, and/or oxide-induced closure).

Aluminum Alloy 2024-T3—Small-crack data [35] have been generated on single-edge-notch tension specimens made of 2024-T3 aluminum alloy (B = sheet thickness = 2.3 mm); and some of these data at R = 0 are shown in Figure 8. Specimens had a notch radius of 3.18 mm and a width (w) of 50 mm. The small-crack data was obtained by using the plastic-replica method. The small-crack data, shown by the symbols, is only a small part of the overall database on this alloy. These results were taken from one laboratory and at an applied stress level of 110 MPa. In the calculation of ΔK for small surface cracks at the notch root, the crack-half-depth-to-crack-length (a/c) ratio was assumed to be 1.0 (see Ref. 35). (Note that for a surface crack at a notch root, the crack depth, 2a, is measured in the sheet thickness, B, direction, and c is measured in the specimen width, w, direction.) This alloy showed a very large difference between the large-crack threshold (about 3 MPa$\sqrt{m}$) [45] and small-crack growth behavior. Small cracks grew at ΔK values as low as 0.75 MPa$\sqrt{m}$. But for ΔK values greater than about 3 MPa$\sqrt{m}$, the small- and large-crack data agreed quite well. The

dashed curve is the ΔK_{eff}-rate (da/dN) relation; and the dashed-dot curve shows the ΔK-rate (dc/dN) relation for large cracks [44]. Although the test data showed a large amount of scatter, the crack-growth analysis (solid curve) from FASTRAN agreed reasonably well with the trends in the test data. The initial 6-μm semi-circular surface defect was very close to the inclusion particle (or void) sizes that initiated cracks at the notch root [35].

Steel 4340—Swain et al [46] conducted small- and large-crack tests on 4340 steel. The large-crack results were obtained on middle-crack tension specimens (B = 5.1 mm) tested at various stress ratios (R = -1, 0 and 0.5). The small-crack data were obtained from single-edge-notch tension (SENT) specimens with a notch radius of 3.2 mm and width w = 25.4 mm (K_T = 3.3) at the same stress ratios. Again, the plastic-replica method was used to measure the growth of small cracks (see Ref. 36). Examination of the initiation sites for 35 fatigue cracks gave information on the distribution of crack-initiation site dimensions. Two types of crack-initiation particles were observed: a spherical particle and a stringer particle, as shown in the SEM photographs in Figures 9(a) and 9(b), respectively. The spherical (calcium-aluminate) particle was by far the most dominant crack-initiation site particle. The cumulative distribution function for these defects is plotted against an equivalent semi-circular defect radius based on the actual area of the defect in Figure 9(c). The mean defect was about 13-μm in radius. Selecting defects of 8- and 30-μm in radius covered over 80% of all defects.

A comparison of some of the small- and large-crack data on the 4340 steel is shown in Figure 10 at the R = 0 condition. The symbols show small surface-crack data from the SENT specimens. The dashed-dot curve is the large-crack data obtained from M(T) specimens [46]. Note that the small cracks were measured in the a-direction and large cracks were measured in the c-direction. Here the small- and large-crack data agreed quite well. The small-crack effect appears to be less dominant at the positive stress-ratio conditions for a variety of materials [35,36]. Again, the dashed curve is the ΔK_{eff}-rate curve determined from the M(T) specimen data. The constraint factor (α) was 2.5 for rates less than 5E-4 mm/cycle [44]. The solid curves show the predicted results from the FASTRAN closure model with either an initial semi-circular surface crack of 8- or 30-μm with S_{max} = 360 MPa. Again, all predictions start on the ΔK_{eff}-rate curve because the initial crack is assumed to be fully open on the first cycle. Because the effective stress-intensity factor curve is near to the large-crack curve, small-crack effects are weak. The predicted results for the largest defect size rapidly approaches the large-crack behavior. But the predicted results for the smallest defect size showed a very rapidly drop and then a very rapid rise to large-crack behavior. Again, this behavior is due to the crack-closure transient and the shape of the ΔK_{eff}-rate curve at low rates.

Prediction of Fatigue Life using Small-Crack Theory

Newman and his co-workers [35-37,41,44,46] have used continuum-mechanics concepts with initial defect sizes, like those which initiated cracks at inclusion particles, voids or slip-bands, and the effective stress-intensity factor range against rate relations to predict the fatigue lives for many engineering materials. The baseline crack-growth rate data for these materials were obtained from large-crack data, in most cases ignoring the large-crack threshold, and using small-crack growth rates at extremely

low rates. Small-crack thresholds were estimated from small-crack data and/or the endurance limits for these materials. In the following, some typical examples of using small-crack theory to predict fatigue behavior will be presented.

Steel 4340—Everett [47,48] conducted fatigue tests on 4340 steel using three types of specimens. The first specimen was an un-notched (K_T = 1) specimen (B = 8.9 mm). The second specimen was the same K_T = 1 specimen but the specimen had a sharp scratch (51-μm deep) machine across the width of the specimen. The last specimen had a single open hole with a radius of 3.2 mm (B = 3.2 mm) that had a stress concentration (K_T) of 3.23. Tests were conducted under both constant-amplitude and spectrum loading. The material used in this study had the same strength level as the material tested in Reference 46 (see Fig. 10), but the specimens had a different thickness and were taken from a different heat of material. However, it was assumed that the large-crack data and inclusion-particle sizes would be the same. A small-crack effective threshold, $(\Delta K_{eff})_{th}$, of 3.2 MPa$\sqrt{m}$ was used to predict the endurance limits or the applied stress level where the initial defect would not grow.

Constant-Amplitude Loading: Figure 11 shows test data obtained from un-notched specimens with and without the machined scratch (solid and open symbols, respectively). All specimens were tested at a stress ratio R = -1. The baseline ΔK_{eff}-rate curve for the steel is shown in Figure 10 (dashed curve). Using the mean defect size from Figure 9, the 13-μm initial semi-circular surface crack, fatigue-life predictions were made on the pristine specimens. The analysis (solid curve) fit the test data quite well. For the specimens with the scratch, an edge-crack configuration was assumed with a crack depth of 51 μm. Using the same baseline data, FASTRAN predicted the influence of the scratch on fatigue life extremely well. These results demonstrate that small-crack theory and the crack-closure model can be used to predict either the influence of either material or manufacturing defects on fatigue life.

Felix-28 Spectrum Loading: Results of fatigue tests conducted under the Felix-28 [49] load sequence are shown in Figure 12 as symbols. The maximum stress in the spectrum is plotted against the cycles to failure. Predictions of total fatigue life under the Felix-28 load spectrum were made using the FASTRAN code [43] by calculating the number of cycles necessary to grow a crack from the assumed initial defect size, located at the center of the open hole, to failure. The predicted results for the two initial defect sizes (8- and 30-μm) bounded the test data quite well.

Aluminum Alloy 2024-T3—In the following, small-crack theory will be used to predict the fatigue life of un-notched laboratory specimens and several types of riveted lap joints with countersunk rivets. The initial crack size will be selected to best fit the experimental test data, like the "equivalent initial flaw size" concept [50].

Laboratory specimens: Grover et al. [51] conducted fatigue tests on flat (K_T = 1) dog-bone specimens made of 2024-T3 aluminum alloy under R = 0 and -1 loading. The specimens were electro-polished but no information on crack-initiation sites was available. Thus, in the analyses it was assumed that cracks initiated as quarter-circular corner cracks. A comparison of experimental and calculated fatigue lives is shown in Figure 13. Various initial crack sizes were

selected by trial-and-error to find the best value to fit the test data. Analyses with a 20-μm initial crack size fit the test data quite well for both R ratios. Results for each R ratio approached the flow stress σ_o (average of the yield stress and ultimate tensile strength) for the high-applied stress levels. Some discrepancies were observed for both R = 0 and -1 analyses at applied stress levels above the yield stress. These discrepancies were expected because the closure model does not account for strain-hardening effects but uses an average flow stress. To fit fatigue limits, a value of $(\Delta K_{eff})_{th}$ of 0.8 MPa$\sqrt{m}$ was needed for the 20-μm initial crack.

Riveted-lap joints: A series of lap-joint tests were conducted by Furuta, Terada and Sashikuma [24] to study the fatigue behavior of countersink riveted lap-joint panels exposed to laboratory air or to a corrosive salt water environment. Figure 14 shows the configuration of the four types of 2024-T3 (Aclad) panels tested: Type 1 - two rivet row, Type 2 - three rivet row, Type 3 - three rivet row with thin-straight tear straps, and Type 4 - three rivet row with non-uniform thick tear straps. The rivet spacing was 20 mm on all joint types, see Figure 2(a) for details on the Type 1 joint. Testing was conducted at constant-amplitude loading which simulated the fuselage skin stress. Tests were conducted under ambient (laboratory air and room temperature) conditions and under a corrosive environment. For the corrosive environment, the lap-joint panels were immersed in circulating 3.5% NaCl solution. Only the results tested in the laboratory air will be considered here (see Ref. 25 for results under the salt solution).

In the FASTRAN code, the riveted-lap-joint analysis used the remote stress due to rivet load (S_p), the by-pass stress (S_b) and the remote bending stresses (S_M) in calculating the stress-intensity factors for a corner crack and through crack emanating from the rivet hole. An interference level (Δ) was not used in the calculations for these panels. Further discussions on why an interference level was not used will be made later. See Figure 3 for illustration of the various rivet loadings. The applied stress, S, was 96 MPa (= $S_p + S_b$) at a stress ratio (R) of 0.125. The two-rivet row (Type 1) panels had a 50% rivet and by-pass stress; whereas, the three-rivet row (Types 2-4) had 37% rivet stress and 63% by-pass stress. Only Type 1 was considered with and without bending, corresponding to panels tested with and without edge clamps to help prevent bending. It was assumed that the tear straps would also help prevent joint bending. Schijve's [52] bending equations (1-degree rivet-rotation correction) were used to estimate the bending stresses for Type 1. Based on 3-D stress analyses presented in Reference 23, the applied stress level of 96 MPa should have yielded the rivet hole and greatly reduced the bending effects.

Furuta et al measured multiple-site cracking on the Type 1 panels. Some typical results on a single panel tested with the edge clamps to prevent joint bending are shown in Figure 15. They used both optical and a SEM examination on the broken specimen to generate the crack length against cycles (open symbols). Cracks initiated and grew at several rivet holes located in the mid-bay of the panel, linked up at about 10 mm half-crack lengths, and caused panel failure. The solid curve is the predicted results from FASTRAN using the baseline ΔK_{eff}-rate curve (Fig. 8) and an initial 6-μm semi-circular flaw. Bending stresses were not considered in these calculations because the panels were restrained from bending with edge clamps. An interference level (Δ) was

not included in these calculations. The 6-μm flaw is the initial defect size needed to predict the fatigue life of pristine circular hole specimens made of this alloy [44]. It was surprising that no interference or clamp-up stresses were needed to predict the life of these panels. In retrospect, if a larger initial flaw size, say a 10-μm flaw, had been assumed, then the fatigue life would have been short of the test data. Then a non-zero interference level would have been required to fit the test data. Thus, it can only be assumed that the 6-μm flaw is an "equivalent initial flaw size" (EIFS) to fit the data. The EIFS accounts for manufacturing defects, rivet interference, clamp-up stresses, and many other features in a lap-joint specimen (see Ref. 25).

Figure 16 shows that the fatigue life of Type 1, 3 and 4 panels tested under ambient (laboratory air and room temperature) conditions (open symbols). Some panels have edge clamps to prevent joint bending and others had tear straps (see Fig. 14). The FASTRAN predictions (solid symbols) agreed well with the panel test results. Here, the fracture mechanics based calculations assumed a 6-μm radius corner crack in a neat-fit rivet-loaded straight shank hole (rivet fit-up and interference fit stresses were assumed small). But at this stage, the 6-μm radius flaw must be considered as an EIFS to account for the many unknowns in a lap-joint panel.

FATIGUE CRACK GROWTH IN METALLIC MATERIALS

Events in the naval, nuclear, and aircraft industries have fostered the development of the field of fracture mechanics and the application of stress-intensity factor analyses to fatigue-crack growth. The failure of the Comet transport jet aircraft [53] from fatigue cracks gave rise to treatments of crack propagation using the stress-intensity factor concept of Irwin [54] and Paris et al [55]. The simplicity of the stress-intensity factor concept rapidly developed into the durability and damage-tolerance concepts currently used today to design fatigue- and fracture-critical components. The discovery of fatigue-crack closure by Elber [56] ushered in a new rational method to treat fatigue-crack growth. The crack-closure concept put crack-propagation theories on a firm foundation and allowed the development of practical life-prediction methods for variable-amplitude and spectrum loading, such as experienced by modern-day commercial aircraft.

In 1968, Elber [56,57] observed that fatigue-crack surfaces contact with each other even during tension-tension cyclic loading. This contact is due to residual plastic deformation that is left in the wake of an advancing crack, as illustrated in Figure 17(a). This deformed material contacts during unloading. It is surprising that this observation appeared so many years after crack growth was first studied. But this simple observation and the explanation of the crack-closure mechanism (or more properly crack-opening) began to explain many crack-growth characteristics almost immediately. Since the discovery of plasticity-induced closure, several other closure mechanisms, such as roughness- and oxide/corrosion/fretting product-induced closure, have been identified. The roughness mechanism, discovered by Walker and Beevers [58], appears to be most prevalent in the near-threshold regime of large-crack growth where the maximum plastic-zone sizes are typically less than the grain size. At these low stress levels, crack extension is primarily along a single slip system resulting in a Stage I-like mechanism and a serrated or zig-zag ($\pm\ \theta$ deg.) crack-

growth path, as shown in Figure 17(b). These cracks will have mixed-mode (Mode I and II) crack-surface deformations, which provide the mechanism for contact between the surfaces during cyclic loading. Suresh and Ritchie [59] have developed a model of roughness-induced closure. Cracks growing along a non-planar path, such as during overloads in aluminum alloys, will develop surface contact and create debris due to fretting and the growth of oxides from the newly created crack surfaces, see Figure 17(c). This debris will cause premature contact, as discussed by Paris et al [60]. These new closure mechanisms, and the influence of the plastic wake on local crack-tip strain field, have greatly advanced the understanding of the fatigue-crack growth process. In the future, models will be developed which will include these three mechanisms of closure, but presently, the majority of the crack-growth models for retardation and acceleration (see Ref. 61 for details) are based on only the plasticity-induced closure concept.

To make life predictions using Elber's crack-closure concept, ΔK_{eff} as a function of the crack-growth rate must be obtained for the material of interest. Fatigue crack-growth rate data should be obtained over the widest possible range in rates (from threshold to fracture), especially if spectrum load predictions are required. Data obtained on the crack configuration of interest would be helpful but it is not essential. The use of the nonlinear crack-tip parameters is only necessary if severe loading (such as low cycle fatigue conditions) is of interest. Most damage-tolerant life calculations can be performed using the linear elastic stress-intensity factor analysis with crack-closure modifications.

Middle-Crack Specimens under Constant-Amplitude Loading

Under constant-amplitude loading, the only unknown in the plasticity-induced crack-closure analysis [42] is the constraint factor, α. The constraint factor accounts for the effects of state-of-stress on crack-tip yielding and crack-surface displacements. The constraint factor is determined by finding (by trial-and-error) a value of α that will correlate the constant-amplitude fatigue-crack-growth-rate data over a wide range in stress ratios, as shown by Newman [62]. This correlation should produce a unique relationship between ΔK_{eff} and crack-growth rate. In the large-crack-growth threshold regime for some materials, the plasticity-induced closure model may not be able to collapse the threshold (ΔK-rate) data onto a unique ΔK_{eff} -rate relation because of other forms of closure. Roughness- and oxide-induced closure (see Ritchie and Lankford [63]) appears to be more relevant in the threshold regime than plasticity-induced closure. This may help explain why the constraint factors needed to correlate crack-growth rate data in the near threshold regime are lower than plane-strain ($\alpha = 3$) conditions. The constraint factors are 1.7 to 2 for aluminum alloys, 1.9 to 2.2 for titanium alloys and 2.5 for steel. Several references [35,37,40 and 41] have shown that large-crack threshold data (determined from the load-reduction procedure) are not applicable for small cracks. However, further study is needed to assess the interactions between plasticity-, roughness- and oxide-induced closure in this regime. If the plasticity-induced closure model is not able to give a unique ΔK_{eff} -rate relation in the threshold regime, then high stress ratio ($R \geq 0.7$) data may be used to help establish the ΔK_{eff} -

rate relation in the near-threshold regime. But small-crack test data should be used to establish the proper ΔK_{eff} -rate relation in the near-threshold regime.

In the following, an illustration of the ΔK_{eff} -rate relation for an aluminum alloy will be presented but similar procedures may be used to establish the relationship for other materials. The large-crack results for 2024-T3 aluminum alloy are shown in Figure 18 for data generated by Hudson [64], Phillips [45] and Dubensky [65]. This figure shows the elastic ΔK_{eff} plotted against crack-growth rate. The data collapsed into a narrow band with several transitions in slope occurring at about the same rate for all stress ratios. Some large differences were observed at high R-ratios in the high-rate regime. These tests were conducted at extremely high remote stress levels (0.75 and 0.95 of the yield stress). Even elastic-plastic crack-tip parameters were unable to collapse the data along a unique curve in this regime. From a high-cycle fatigue standpoint, however, this discrepancy has very little influence on total life. The elastic-plastic fracture criterion (Two-Parameter Fracture Criterion, TPFC; see Ref. 66) used in the analysis (K_F = 267 MPa$\sqrt{m}$; m = 1) predicted failure very near to the vertical asymptotes of the test data, see the vertical dashed and dotted lines for R = 0.7 and 0.5 (at 0.75 and 0.95 of yield), respectively. Similar vertical lines (not shown) would also indicate failure at the other R ratios. Lower R ratios would fail at higher values of ΔK_{eff}. For these calculations, a constraint factor (α) of 2.0 was used for rates less than 1E-07 m/cycle (start of transition from flat-to-slant crack growth) and α equal to 1.0 was used for rates greater than 2.5E-06 m/cycle (end of transition from flat-to-slant crack growth). For intermediate rates, α was varied linearly with the logarithm of crack-growth rate (see Ref. 43). The values of α and rate were selected by trial-and-error and from analyses of crack growth under spectrum loading (see Ref. 67). The constraint-loss regime (α = 2 to 1) has also been associated with the flat-to-slant crack-growth behavior. Reference 67 developed an expression to predict the location of the flat-to-slant crack-growth regime and the effective stress-intensity factor at transition is by

$$(\Delta K_{eff})_T = 0.5\ \sigma_o\ \sqrt{B} \qquad (1)$$

For the 2024-T3 alloy sheet, $(\Delta K_{eff})_T$ = 10.2 MPa$\sqrt{m}$. The width of the constraint-loss regime, in terms of rate or ΔK_{eff}, is a function of thickness but this relationship has yet to be developed. In the low crack-growth rate regime, near and at threshold, tests and analyses [40,68] have indicated that the threshold develops because of a rise in the crack-opening-stress-to-maximum-stress ratio due to the load-shedding procedure. In the threshold regime then, the actual ΔK_{eff} -rate data would lie at lower values of ΔK_{eff} because the rise in crack-opening stress was not accounted for in the current analysis. For the present study, an estimate was made for this behavior on the basis of small-crack data [35] and it is shown by the solid line below rates of about 2E-09 m/cycle. The baseline relation shown by the solid line was used to predict fatigue lives under constant-amplitude results shown in Figures 13, 15 and 16.

Middle-Crack Specimens under Spectrum Loading

Wanhill [69] conducted spectrum crack-growth tests on middle-crack tension specimens made of 2024-T3 Alclad material (B = 3.1 mm). Tests were conducted under the TWIST (transport wing spectrum) [70] clipped at Level III with a mean flight stress of S_{mf} = 70 MPa. Figure 19 shows a comparison of test results and calculated results from Newman's closure model [42,43] with the constraint-loss regime (α = 2 to 1) estimated from equation (1). The model used ΔK_{eff}-rate data like that shown in Figure 18, but for the 2024-T3 Alclad alloy. To illustrate why the constraint-loss regime is necessary, example calculations were made for constant constraint conditions of either α = 1 or 2 (dashed curves). The model with a low constraint condition (α = 1) predicted much longer lives than the tests, whereas the model with the high constraint predicted much shorter lives than the tests. Thus, the correct constraint-loss regime is required to predict fatigue-crack growth under aircraft spectrum loading in thin-sheet materials.

Stiffened Panels under Constant-Amplitude Loading

In 1971, Poe [71] conducted fatigue-crack growth tests on riveted-stiffened panels made of 2024-T3 sheet material with either aluminum or steel stiffeners. The dimensions of the panel are shown in Figure 20. The total width (2w) of the panel was 915 mm. The panel had five intact stiffeners with a single crack located under the central stiffener. The stringers were placed symmetrical about the sheet, so that sheet bending would be minimized. Poe had also developed a stress-analysis code to determine the stress-intensity factors for a crack in an infinite sheet with stiffeners attached with rigid fasteners. The normalized stress-intensity factor against crack-length-to-half-width (c/w) ratio is shown in Figure 21, as the solid curve. These results were for a stiffened panel that had a stringer-area-to-total-area (μ) ratio of 0.41. These results showed that the normalized stress-intensity factor dropped rapidly as the crack approaches a stringer (located at c/w = 0.33 and 0.66). In 1999, Chen [72] conducted a stress analysis of Poe's panel but assumed that the fasteners were flexible using Swift's fastener-flexibility model [3]. Because of the more flexible fasteners and lower fastener loads, Chen's stress-intensity factors (dashed curve) were 10 to 20% higher than Poe's solution.

The experimental results obtained from two panels tested by Poe [71] under constant-amplitude fatigue loading with a remote applied stress of 103 MPa at R = 0.1 are shown in Figure 22. This figure shows crack length against crack-growth rate measured (symbols) from two panels with μ = 0.41. These results show higher rates for large crack lengths until the crack approaches the first stiffener. Here the rates show a rapid drop and then rise after the crack grows pass the stiffener. FASTRAN and the ΔK_{eff}-rate curve shown Figure 18 were used to make several predictions. First, the dotted curve shows the predictions made for an un-stiffened panel. These results predict much higher rates than the tests. Using Poe's stress-intensity factor solution (Fig. 21), the predictions are shown as the dashed curve. Here the predicted rates agreed for crack lengths less that about 25 mm but the predicted rates were 20 to 40% lower than the measured rates for larger crack lengths. Using Chen's stress-intensity factor solution (Fig. 21), the predictions are shown as the solid curve. The predicted results agreed quite well with the measured rates except for the

largest crack lengths (c > 150 mm). It is suspected that rivet yielding or fastener-hole yielding, which was not accounted for in the either analysis, would have caused lower rivet loads and, consequently, higher crack-growth rates. These results demonstrate that rivet flexibility is an important parameter to consider when predicting the fatigue crack growth or fracture behavior of stiffened panels.

FRACTURE OF METALLIC MATERIALS

One of the objectives of the NASA Airframe Structural Integrity Program [7] was to develop the methodology to predict the residual strength of fuselage structures with large two-bay cracks in the presence of multiple-site damage (MSD) cracking at adjacent rivet holes. The prediction of the residual strength of a complex built-up shell structure, such as a fuselage with frames, tear-straps, and lap-splice joints, required the integration of a ductile fracture criterion and a detailed nonlinear stress analysis of the cracked structure. The critical crack-tip opening-angle (CTOA) fracture criterion [73-75] has been experimentally verified to be a valid fracture criterion for mode I stress states in thin and moderately thick (13-mm or less) aluminum alloys [76-78]. The CTOA criterion has been demonstrated to be valid for predicting the link-up of a large lead crack with small fatigue cracks ahead of the advancing lead crack [79]. This fracture criterion has been implemented into the STAGS geometric and material nonlinear finite-element-based shell analysis code [12] to provide an integrated structural-integrity analysis methodology. The capability to model a growing crack that may extend in a non-self-similar direction has been added to the FRANC3D/STAGS code [80] along with an automated mesh refinement and adaptive remeshing procedure. The topological description of the growing crack is provided by the FRANC3D fracture mechanics code. The geometric nonlinear behavior of a stiffened fuselage shell is currently under study for internal pressure loads combined with fuselage body loads that produce tension, compression and shear loads in the shell.

In the following sections, the CTOA fracture criterion will be reviewed and some experimental measurements will be presented on a fuselage material. The application of two-dimensional finite-element analyses to simulate the fracture process using the critical CTOA will be presented to illustrate how the state-of-stress (plane-stress or plane-strain conditions) around the crack front affects the fracture analysis. In practice, wide panel fracture tests are usually conducted with anti-buckling guide plates to prevent the out-of-plane deformations of the crack. But restraining the out-of-plane deformations have been found to be very difficult, especially for wide panels with stringers or tear-straps. Because large 2-bay cracks in fuselage structure exhibit large out-of-plane deformations (bulging from internal pressure), the analysis tools must be able to predict the influence of bulging or buckling on the fracture process. Thus, the use of anti-buckling guide plate systems should be used only in limited cases and the wide panels should be allowed to buckle, so that experimental test data can be obtained with both in-plane and out-of-plane deformations. The use of the STAGS shell code to predict the fracture behavior under these conditions will be illustrated. The application of the STAGS/CTOA analysis will be presented on some of the FAA/NASA wide panel fracture tests [81]. These tests combined the influence of a large lead crack with various sizes of multiple-site damage (MSD) cracking (simulating a rivet-row

cracking), with intact or broken stiffeners, and severe out-of-plane deformations during stable tearing, crack link-up, and fracture.

CTOA Fracture Criterion

The critical crack-tip-opening-angle (CTOA) fracture criterion is a "local" approach to characterizing fracture. An extensive test program [82] has been conducted to experimentally study the characteristics of the CTOA criterion and to establish its validity as a fracture criterion for thin-sheet 2024-T3. Several laboratory-type specimens have been used to measure the CTOA during the fracture process. A high-resolution long-focal-length microscope was used to record the stable-tearing results. The tearing event was then analyzed on a frame-by-frame basis and CTOA was measured, as shown in Figure 23. Measurements made on compact C(T) and various size middle-crack tension M(T) specimens are shown in Figure 24. The critical CTOA was relatively insensitive to crack extension after an initial transition region. The initial transition region has been traced to 3D effects that occur as the crack tunnels and transitions from flat-to-slant crack growth [78]. Three-dimensional fracture simulations with stable tearing and tunneling have demonstrated that the CTOA is high at the free surface and rapidly drops during crack extension [83]. But the CTOA in the interior is low and rises during stable tearing. After a small amount of stable tearing (about equal to sheet thickness), the critical CTOA in the interior and at the free surface approach nearly the same value. Over 50 mm of stable tearing was recorded and the CTOA values were nearly constant (5.8 degs.).

Two-Dimensional Finite-Element Analyses with Plane-Strain Core

In the past [74-75], two-dimensional (2D) elastic-plastic finite-element analyses, under plane-stress conditions, were used to study stable tearing in an aluminum alloy (6-mm thick). But the results indicated that CTOA was high at crack initiation and dropped with crack extension. The drop was not as rapid as that shown in Figure 24. The results were discouraging and indicated that CTOA was not a constant. However, Newman et al [77] found that neither plane-stress nor plane-strain conditions were able to fit experimental test data (25-mm thick steel) using the critical CTOD fracture criterion (equivalent to the CTOA criterion). But a hybrid analysis with a core of plane-strain elements around the crack tip and plane-stress elements elsewhere was able to fit the test data quite well.

The influence of the state-of-stress on fracture is illustrated in Figure 25. Fracture results from various width middle-crack tension specimens (restrained from buckling) are shown as symbols [84]. The failure stress is plotted against specimen width for $2c/W = 1/3$. By trial-and-error and using the 2D elastic-plastic finite-element analysis, a critical angle (ψ_c) of 4.7 degrees with a plane-strain core of 1.9 mm was determined to best fit the data (solid curve). The plane-strain core half-height (h_c) is measured from the crack plane to the height of the core. Elements within this core had plane-strain conditions. The upper dash-dot curve shows the calculations made with all plane-stress elements and $\psi_c = 4.7$ degrees. The shape of the curve is such that it would not be able to fit the failure stresses on all of the specimens. Likewise, the dashed curve is the results

of plane-strain analyses. Here the analyses fit the smaller specimens but under predicts the failure stresses on the large specimens. Thus, the fracture process is a 3D problem and the use to the "plane-strain core" concept allows 2D analyses to accurately simulate the fracture process. The plane-strain core (h_c about equal to the thickness) models the high constraint around a crack tip but allows for the widespread plastic yielding under plane-stress conditions away from the crack tip.

Effects of Buckling and Various Anti-Buckling Guide Systems

The use of guide plates is intended to decouple the crack-growth process from buckling behavior. The intent is to determine the load-crack-extension behavior under restrained conditions. A series of wide panel tests (1000-mm wide) were conducted by Dawicke et al [85] to determine the effects of various guide plate systems on residual strength. The first two tests were conducted without guide plates, Figure 26(a), and the average failure stress was 166 MPa. The applied stress against crack extension for these two tests are shown in Figure 27 as the lowest symbols. The initial 1000-mm wide guide plates consisted of four 12.7-mm-thick sheets of aluminum alloy that sandwiched the specimen. Teflon sheets were placed between the guide plates and the specimen to reduce the friction between the specimen and guides. The 1000-mm wide specimen tested with these guide plates experienced a 24% increase in failure stress over the unconstrained test, as shown in Figure 26(a) and the square symbols in Figure 27. The guide plate system shown in Figure 26(b) had been sufficient to prevent buckling in smaller width specimens, but the guide plates alone did not prevent buckling in the 1000-mm wide panel. The guide plates were observed to deform out-of-plane about 3 mm, indicating that the stiffness of the guide plates was not sufficient to prevent buckling. The out-of-plane stiffness of the guide plates was increased by attaching six pairs of I-beams to the outside of the plates, as shown in Figure 26(c). A third, identical specimen was tested with the modified guide plate system and the measured failure stress was 46% higher than the unconstrained test. A comparison of the applied stress against crack extension for the unrestrained tests and the other tests conducted with the two guide plate systems are shown in Figure 27.

The STAGS shell code [12] and the critical CTOA fracture criterion has been used to study the behavior of cracked panels that were either restrained from buckling or allow to buckle [86]. It has been found that the same CTOA can be used to predict the effects of buckling on stable tearing. An illustration of the STAGS/CTOA capability is shown in Figure 28. Two middle-crack tension panels (W = 610 mm wide) were tested with anti-buckling guides [87] and these results are shown as the upper most symbols. Then two identical crack panels were tested without the guides [87] and these results are shown as the lower symbols. Buckling had a large influence (about 25%) on the residual strength. The critical CTOA (ψ_c) of 5 degrees was determined from a ZIP3D fracture analysis and the plane-strain core height (h_c) of 1 mm was determined from a ZIP2D fracture analysis (to fit the ZIP3D results) from 152-mm wide compact tension specimen tests [88]. The ψ_c and h_c values were then used in the STAGS code (with the plane-strain core option [12]) to predict stable tearing on the panel restrained from buckling (dashed curve) and the

panel allowed to buckle (solid curve). The predicted results agreed quite well with the test data and demonstrate that the fracture methodology can account for severe out-of-plane deformations. This methodology has been successful used to predict stable tearing and residual strength in large curved pressured fuselage test articles within about 10% [88].

FAA/NASA Wide Panel Fracture Tests

NASA and the FAA jointly designed and conducted fracture tests on 1016-mm wide sheets made of 1.6-mm thick 2024-T3 aluminum alloy with and without stiffeners [81]. Some of the specimens had five 7075-T6 aluminum alloy stiffeners (2.2-mm thick) riveted on each side of the sheet, as shown in Figure 29. The central stiffeners were cut along the crack line. Open holes were machined into the sheet at the required rivet spacing along the crack line but rivets were not installed. Five different crack configurations were tested: a single center crack, a single center crack with an array of 12 holes on either side of the lead crack, and a single center crack with three different equal MSD cracking (0.25, 0.76 and 1.3-mm) at the edge of each hole, see Reference 89. For each crack configuration, identical specimens were tested with and without riveted stringers. All tests were conducted under stroke control. Measurements were made of load against crack extension.

Comparisons of measured and predicted load against crack extension for a stiffened panel test with a single crack and a test with a single crack and MSD are shown in Figures 30(a) and 30(b), respectively. The CTOA (ψ_c = 5.4 deg.) was determined from laboratory specimens restrained from buckling [89]. The stiffened panels were allowed to buckle. The STAGS analyses with the plane-strain core (h_c = 2 mm) compared extremely well with the test data (symbols). These results demonstrate that the residual-strength analysis method can predict stable crack growth and failure loads for complex structure.

CONCLUDING REMARKS

The Seventeenth Frederik J. Plantema Memorial Lecture presented a review of some of the technical developments and concepts that have led to a better understanding of the fatigue and fracture process in metallic materials. Advances in computer technology has allowed more accurate stress analyses to be conducted on three-dimensional crack configurations, more realistic simulations of the fatigue process and fatigue-crack growth in structural components, and the use of more advanced elastic-plastic fracture mechanics concepts to assess the residual strength and fail-safe capability of aircraft structures. The following conclusions were drawn from this review:

(1) Finite-element and boundary-element analyses are able to determine accurate stress-intensity factors for cracked structural components.

(2) "Fatigue" is "crack propagation" from micro-structural features, such as inclusion particles, voids, and slip bands, for many engineering materials; and fatigue lives can be predicted under constant- and variable-amplitude loading with Small-Crack Theory.

(3) Fatigue-crack growth can be predicted under aircraft spectrum loading with the Crack-Closure Concept and consideration of constraint effects on plastic yielding around the crack.

(4) Fracture of "thin-sheet" materials under the influence of riveted stringers, buckling, and multiple-site damage cracking can be predicted with the critical crack-tip-opening-angle (CTOA) fracture criterion.

REFERENCES

[1] Schijve, J., "Fatigue Life of Structural Components under Random Loading," 2nd Plantema Memorial Lecture, International Committee on Aeronautical Fatigue (ICAF), Stockholm, Sweden, 1969.

[2] Goranson, U. G, "Damage Tolerance – Facts and Fiction," 14th Plantema Memorial Lecture, 17th Symposium of the International Committee on Aeronautical Fatigue (ICAF), Stockholm, Sweden, June 9, 1993.

[3] Swift, T., "Damage Tolerance in Pressurized Fuselage," 11th Plantema Memorial Lecture, 14th Symposium of the International Committee on Aeronautical Fatigue (ICAF), New Materials and Fatigue Resistant Aircraft Design, Ottawa, Canada, June 8-12, 1987.

[4] Structural Integrity of Aging Airplanes, S. N. Atluri; S. G. Sampath and P. Tong, eds., Springer-Verlag, 1991.

[5] FAA-NASA Symposium on the Continued Airworthiness of Aircraft Structures, C. A. Bigelow, ed., DOT/FAA/AR-97/2, July 1997.

[6] The Second Joint NASA/FAA/DoD Conference on Aging Aircraft, C. E. Harris, ed., NASA CP-208982, January 1999.

[7] Harris, C. E.; Newman, J. C., Jr.; Piascik, R. and Starnes, J. H., Jr., "Analytical Methodology for Predicting the Onset of Widespread Fatigue Damage in Fuselage Structure," Journal of Aircraft, Vol. 35, No. 2, 1998, pp. 307-317.

[8] ABAQUS User's Manuals, Version 5.5, Hibbitt, Karlsson and Sorensen, Inc., 1995.

[9] ANSYS User's Manuals, Version 5.4, Swanson Analysis Systems, Inc., 1998.

[10] MSC/NASTRAN User's Manuals, Version 70.5, MacNeal-Schwendler Corp., 1999.

[11] Almroth, B; Brogan, F. and Stanley, G., "User's Manual for STAGS," NASA CR-165670, 1978.

[12] Rankin, C. C.; Brogan, F. A.; Loden, W. A. and Cabiness, H. D., "STAGS User Manual – Version 2.4," Lockheed Martin Advanced Technology Center, Report LMSC P032594, 1997.

[13] Newman, J. C., Jr., "Finite-Element Analysis of Fatigue Crack Propagation – Including the Effects of Crack Closure," Ph. D. Thesis, Virginia Polytechnic Institute and State University, Blacksburg, VA, May 1974.

[14] Raju, I. S. and Newman, J. C., Jr., "surf3d: A 3-D Finite-Element Program for the Analysis of Surface and Corner Cracks in Solids subjected to Mode-I Loadings," NASA TM-107710, February 1993.

[15] Shivakumar, K. N. and Newman, J. C., Jr., "ZIP3D – An Elastic and Elastic-Plastic Finite-Element Analysis Program for Cracked Bodies," NASA TM-102753, November 1990.
[16] Chang, C. C. and Mear, M. E., "A Boundary Element Method for Two-Dimensional Linear Elastic Fracture Analysis," International Journal of Fracture, Vol. 74, 1996, pp. 219-251.
[17] Wawrzynek, P. and Ingraffea, A., "FRANC2D: A Two-Dimensional Crack Propagation Simulator," NASA CR-4572, March 1994.
[18] Potyondy, D. O.; Wawrzynek, P. A. and Ingraffea, A. R., "Discrete Crack Growth Analysis Methodology for Through Cracks in Pressurized Fuselage Structures," NASA CP-3274, C. E. Harris, ed., September 1994, pp. 581-602.
[19] Koppenhoefer, K. C., Gullerud, A. S., Ruggieri, C. and Dodds, R. H., Jr., "WARP3D: Dynamic Nonlinear Analysis of Solids using a Preconditioned Conjugate Gradient Software Architecture," Structural Research Series (SRS) 596, UILU-ENG-94-2017, University of Illinois at Urbana-Champaign, 1994.
[20] Young, R. D.; Rouse, M.; Ambur, D. R. and Starnes, J. H., Jr., "Residual Strength Pressure Tests and Nonlinear Analyses of Stringer- and Frame-Stiffened Aluminum Fuselage Panels with Longitudinal Cracks," The Second Joint NASA/FAA/DoD Conference on Aging Aircraft, C. E. Harris, ed., NASA CP-208982, 1999, pp. 408-426.
[21] Chen, C. S.; Wawrzynek, P. A. and Ingraffea, A. R., "Crack Growth Simulation and Residual Strength Prediction in Airplane Fuselages," NASA/CR-1999-209115, March 1999.
[22] Hartman, A., "The Influence of Manufacturing Procedures on the Fatigue of 2024-T3 Alclad Riveted Single Lap Joints," NLR TR 68072 U, July 1968.
[23] Newman, J. C., Jr.; Harris, C. E.; James, M. A. and Shivakumar, K. N., "Fatigue-Life Prediction of Riveted Lap-Splice Joints using Small-Crack Theory," Fatigue in New and Ageing Aircraft, R. Cook and P. Poole, eds., EMAS, Ltd., 1997, pp. 523-552.
[24] Furuta, S.; Terada, H. and Sashikuma, H., "Fatigue Strength of Fuselage Joint Structures under Ambient and Corrosive Environment," Fatigue in New and Ageing Aircraft, R. Cook and P. Poole, eds., EMAS, Ltd., 1997, pp. 231-249.
[25] Harris, C. E.; Newman, J. C., Jr. and Piascik, R. S., "A Practical Engineering Approach to Predicting Fatigue Crack Growth in Riveted Lap Joints," 20th Symposium of the International Committee on Aeronautical Fatigue (ICAF), Bellevue, WA, July 14-16, 1999.
[26] Piascik, R. S.; Willard, S. A. and Miller, M., "The Characterization of Widespread Fatigue Damage in Fuselage Structure," FAA/NASA International Symposium on Advanced Structural Integrity Methods for Airframe Durability and Damage Tolerance, NASA CP-3274, 1994, pp. 563-580.
[27] Piascik, R. S. and Willard, S. A., "The Characteristics of Multi-Site Fatigue Damage in the Fuselage Riveted Lap Splice Joint," Fatigue in New and Ageing Aircraft, R. Cook and P. Poole, eds., EMAS, Ltd., 1997, pp. 93-114.
[28] Newman, J. C., Jr., "A Review and Assessment of the Stress-Intensity Factors for Surface Cracks," Part-Through Crack Fatigue Life Prediction, ASTM STP 687, J. B. Chang, ed., American Society for Testing and Materials, Philadelphia, PA, 1979, pp. 16-42.
[29] Raju, I. S. and Newman, J. C., Jr., "Stress-Intensity Factors for a Wide Range of Semi-Elliptical Surface Cracks in Finite-Thickness Plates," Engineering Fracture Mechanics, Vol. 11, No. 4, 1979, pp. 817-829.
[30] Bakuckas, J. G., Jr., "Comparison of Boundary Correction Factor Solutions for Two Symmetric Cracks in a Straight-Shank Hole," DOT/FAA/AR-98/36, April 1999.

[31] Raju, I. S. and Newman, J. C., Jr., "Stress-Intensity Factors for Two Symmetric Corner Cracks," Fracture Mechanics, ASTM STP 677, C. W. Smith, eds., American Society for Testing and Materials, 1979, pp. 411-430.
[32] Gullerud, A. S.; Dodds, R. H., Jr.; Hampton, R. W. and Dawicke, D. S., "3-D Finite Element Modeling of Ductile Crack Growth in Thin Aluminum Materials," Fatigue and Fracture Mechanics: 30th Volume, K. L. Jerina and P. C. Paris, eds., American Society for Testing and Materials, 1998.
[33] Helm, J. D., "Use of Three-Dimensional Digital Image Correlation for the Experimental Characterization of Buckling in Large, Thin, 2024-T3 Aluminum, Middle-Crack Tension Specimens," Ph. D. Thesis, University of South Carolina, 1999.
[34] Schijve, J., "Four Lectures on Fatigue Crack Growth," Engineering Fracture Mechanics, Vol. 11, 1979, pp. 167-221.
[35] Newman, J. C., Jr. and Edwards, P. R., "Short-Crack Growth Behaviour in an Aluminum Alloy – and AGARD Cooperative Test Programme," AGARD R-732, 1988.
[36] Short-Crack Growth Behaviour in Various Aircraft Materials, P. R. Edwards and J. C. Newman, Jr., eds., AGARD R-767, 1990.
[37] Newman, J. C., Jr., Wu, X. R., Venneri, S. and Li, C., "Small-Crack Effects in High-Strength Aluminum Alloys," NASA RP-1309, 1994.
[38] Pearson, S., "Initiation of Fatigue Cracks in Commercial Aluminum Alloys and the Subsequent Propagation of Very Short Cracks," Engineering Fracture Mechanics, Vol. 7, No. 2, 1975, pp. 235-247.
[39] Lankford, J., "The Growth of Small Fatigue Cracks in 7075-T6 Aluminum," Fatigue of Engineering Materials and Structures, Vol. 5, 1982, pp. 233-248.
[40] Newman, J. C, Jr., "A Nonlinear Fracture Mechanics Approach to the Growth of Small Cracks," Behaviour of Short Cracks in Airframe Components, H. Zocher, ed., AGARD CP-328, 1983, pp. 6.1-6.26.
[41] Newman, J. C., Jr., Swain, M. H. and Phillips, E. P., "An Assessment of the Small-Crack Effect for 2024-T3 Aluminum Alloy," Small Fatigue Cracks, The Metallurgical Society, Inc., Warrendale, PA, 1986, pp. 427-452.
[42] Newman, J. C., Jr., "A Crack Closure Model for Predicting Fatigue Crack Growth under Aircraft Spectrum Loading," Methods and Models for Predicting Fatigue Crack Growth under Random Loading, J. B. Chang and C. M. Hudson, eds., ASTM STP 748, 1981, pp. 53-84.
[43] Newman, J. C., Jr., "FASTRAN II – A Fatigue Crack Growth Structural Analysis Program," NASA TM 104159, 1992.
[44] Newman, J. C., Jr.; Phillips, E. P. and Swain, M. H., "Fatigue-Life Prediction Methodology using Small-Crack Theory," International Journal of Fatigue, Vol. 21, 1999, pp. 109-119.
[45] Phillips, E. P., "The Influence of Crack Closure on Fatigue Crack Growth Thresholds in 2024-T3 Aluminum Alloy," Mechanics of Fatigue Crack Closure, ASTM STP 982, J. C. Newman, Jr. and W. Elber, eds., American Society for Testing and Materials, Philadelphia, PA, 1988, pp. 505-515.
[46] Swain, M. H.; Everett, R. A.; Newman, J. C., Jr. and Phillips, E. P., "The Growth of Short Cracks in 4340 Steel and Aluminum-Lithium 2090," AGARD R-767, 1990, pp. 7.1-7.30.

[47] Everett, R. A., Jr.; Newman, J. C., Jr. and Phillips, E. P., “The Effects of Machining-Like Scratch on the Fatigue Life of 4340 Steel”, Proceedings of the American Helicopter Society, 55th Annual Forum, Montreal, Quebec, Canada, May 25-27, 1999.
[48] Everett, R. A., Jr., “A Comparison of Fatigue Life Prediction Methodologies for Rotorcraft,” NASA TM 102759, 1990.
[49] Edwards, P. R. and Darts, J., “Standardised Fatigue Loading Sequences for Helicopter Rotors (Helix and Felix),” Royal Aircraft Establishment, Technical Report 84084, August 1984.
[50] Rudd, J. L., Yang, J. N., Manning, S. D. and Garver, W. R., "Durability Design Requirements and Analysis for Metallic Structures," Design of Fatigue and Fracture Resistant Structures, ASTM STP 761, P.R. Abelkis and C.M. Hudson, eds., 1982, pp. 133-151.
[51] Grover, H. J.; Hyler, W. S.; Kuhn, P.; Landers, C. B. and Howell, F. M., “Axial-Load Fatigue Properties of 24S-T and 75S-T Aluminum Alloy as Determined in Several Laboratories,""NACA TN-2928, 1953.
[52] Schijve, J., “Some Elementary Calculations on Secondary Bending in Simple Lap Joints,” NLR TR 72036 U, 1972.
[53] Cohen, B, Farren, W., Duncan, W. and Wheeler, A., “Report of the Court of Inquiry into the Accidents to Comet G-ALYP on 10 January 1954 and Comet G-ALYY on 8 April 1954,” HMSO, London, 1955.
[54] Irwin, G. R., “Analysis of Stresses and Strains near the End of a Crack Tranversing a Plate,” Journal of Applied Mechanics, Vol. 24, 1957, pp. 361-364.
[55] Paris, P., Gomez, M. and Anderson, W. A., “A Rational Analytic Theory of Fatigue,” Trend in Engineering, Vol. 13, 1961, pp. 9-14.
[56] Elber, W., “Fatigue Crack Propagation,” Ph.D. Thesis, University of New South Wales, 1968.
[57] Elber, W., “The Significance of Fatigue Crack Closure,” Damage Tolerance in Aircraft Structures, ASTM STP 486, 1971, pp. 230-242.
[58] Walker, N. and Beevers, C. J., “A Fatigue Crack Closure Mechanism in Titanium,” Fatigue of Engineering Materials and Structures, Vol. 1, No. 1, 1979, pp. 135-148.
[59] Suresh, S. and Ritchie, R. O., “A Geometric Model for Fatigue Crack Closure Induced by Fracture Surface Roughness,” Metal Transactions, Vol. A13, 1982, pp. 1627-1631.
[60] Paris, P. C., Bucci, R. J., Wessel, E. T., Clark, W. G. and Mager, T. R., “Extensive Study of Low Fatigue Crack Growth Rates in A533 and A508 Steels,” ASTM STP 513, 1972, pp. 141-176.
[61] Newman, J. C., Jr., “The Merging of Fatigue and Fracture Mechanics Concepts: A Historical Perspective,” Progress in Aerospace Sciences, Vol. 34, No. 5-6, 1998, pp. 345-388.
[62] Newman, J. C., Jr., “A Crack-Opening Stress Equation for Fatigue Crack Growth,” International Journal of Fracture, Vol. 24, 1984, pp. R131-R135.
[63] Small Fatigue Cracks, Ritchie, R. O. and Lankford, J., eds., The Metallurgical Society, Inc., Warrendale, PA, 1986.
[64] Hudson, C. M., “Effect of Stress Ratio on Fatigue-Crack Growth in 7075-T6 and 2024-T3 Aluminum Alloy Specimens,” NASA TN D-5390, 1969.

[65] Dubensky, R. G., "Fatigue Crack Propagation in 2024-T3 and 7075-T6 Aluminum Alloys at High Stress," NASA CR-1732, March 1971.
[66] Newman, J. C., Jr., "Fracture Analysis of Various Cracked Configurations in Sheet and Plate Materials," ASTM STP 605, 1976, pp. 104-123.
[67] Newman, J. C., Jr., "Effects of Constraint on Crack Growth under Aircraft Spectrum Loading," Fatigue of Aircraft Materials, A. Beukers et al, eds., Delft University Press, 1992, pp. 83-109.
[68] Minakawa, K. and McEvily, A. J., "On Near-Threshold Fatigue Crack Growth in Steels and Aluminum Alloys," Proceedings of the International Conference on Fatigue Thresholds, Vol. 2, 1981, pp. 373-390.
[69] Wanhill, R. J. H., "Flight Simulation Fatigue Crack Propagation Evaluation of Candidate Lower Wing Skin Materials with Particular Consideration of Spectrum Truncation," NLR TR 77092 U, July 1977.
[70] deJonge, J. B., Schutz, D., Lowak, H. and Schijve, J., "A Standard Load Sequence for Flight Simulation Tests on Transport Aircraft Wing Structures (TWIST)," NLR TR-73029 U, Nationaal Lucht-en Ruimtevaartlaborium, Netherlands, 1973.
[71] Poe, C. C., Jr., "Stress-Intensity Factor for a Cracked Sheet with Riveted and Uniformly Spaced Stringers," NASA TR R-358, May 1971.
[72] Chen, C., Private communication, The Boeing Company, Long Beach, CA., February 1999.
[73] deKoning, A. U., "A Contribution to the Analysis of Slow Stable Crack Growth," National Aerospace Laboratory Report NLR MP 75035U, The Netherlands, 1975.
[74] Kanninen, M. F.; Rybicki, E. F.; Stonesifer, R. B., Broek, D.; Rosenfield, A. R.; Marschall, C. W. and Hahn, G. T., "Elastic-Plastic Fracture Mechanics for Two-Dimensional Stable Crack Growth and Instability Problems", Elastic-Plastic Fracture, ASTM STP 668, American Society for Testing and Materials, Philadelphia, PA, 1979, pp. 121-150.
[75] Shih, C. F.; de Lorenzi, H. G. and Andrews, W. R., "Studies on Crack Initiation and Stable Crack Growth", Elastic-Plastic Fracture, ASTM STP 668, American Society for Testing and Materials, Philadelphia, PA, 1979, pp. 65-120.
[76] Newman, J. C., Jr., "An Elastic-Plastic Finite-Element Analysis of Crack Initiation, Stable Crack Growth and Instability," ASTM STP 833, American Society for Testing and Materials, Philadelphia, PA, 1984, pp. 93-117.
[77] Newman, J. C., Jr.; Booth, B. C. and Shivakumar, K. N., "An Elastic-Plastic Finite-Element Analysis of the J-Resistance Curve using a CTOD Criterion," Fracture Mechanics: Eighteenth Symposium, ASTM STP 945, D. T. Read and R. P. Reed, eds., American Society for Testing and Materials, Philadelphia, PA, 1988, pp. 665-685.
[78] Newman, J. C., Jr.; Bigelow, C. A. and Dawicke, D. S., "Finite-Element Analyses and Fracture Simulation in Thin-Sheet Aluminum Alloy," Durability of Metal Aircraft Structures, S. N. Atluri et al, eds., W. H. Wolfe Associates, Alpharetta, GA., 1992, pp. 167-186.
[79] Newman, J. C., Jr.; Dawicke, D. S.; Sutton, M. A.; and Bigelow, C. A., "A Fracture Criterion for Widespread Cracking in Thin-Sheet Aluminum Alloys", Durability and Structural Integrity of Airplanes, Vol. I, A. F. Blom, ed., EMAS Ltd., 1993, pp. 443-468.
[80] Potyondy, D. O.; Wawrzynek, P. A.; and Ingraffea, A. R., "Discrete Crack Growth Analysis Methodology for Through Cracks in Pressurized Fuselage Structures," NASA CP 3274, C. E. Harris, ed., 1994, pp. 581-602.

[81] Dawicke, D. S.; Newman, J. C., Jr. and Tan, P. W., "FAA/NASA Wide Panel Fracture Tests – Part I Executive Summary," NASA TP (in progress), 1999.
[82] Dawicke, D. S.; Sutton, M. A.; Newman, J. C, Jr. and Bigelow, C. A., "Measurement and Analysis of Critical CTOA for an Aluminum Alloy Sheet," Fracture Mechanics: Twenty-Fifth Volume, ASTM STP 1220, F. Erdogan, ed., 1995, pp. 358-379.
[83] Dawicke, D. S.; Newman, J. C.; and Bigelow, C. A., "Three-Dimensional CTOA and Constraint Effects during Stable Tearing in a Thin-Sheet Material," Fracture Mechanics: 26th Volume, ASTM STP 1256, W. G. Reuter, J. H. Underwood and J. C. Newman, Jr., eds., 1995, pp. 223-242.
[84] Eichenberger, T. W., "Fracture Resistance Data Summary," Report DA-20947, The Boeing Company, June 1992.
[85] Dawicke, D. S.; Gullerud, A. S.; Dodds, R. H., Jr.; and Hampton, R. W., "Residual Strength Predictions with Crack Buckling," The Second Joint NASA/FAA/DoD Conference on Aging Aircraft, C. E. Harris, ed., NASA CP-208982, 1999, pp. 565-574.
[86] Seshadri, B. R. and Newman, J. C., Jr., "Analysis of Buckling and Stable Tearing in Thin-Sheet Materials," Fatigue and Fracture Mechanics: 29th Volume, ASTM STP 1332, T. L. Panontin and S. D. Sheppard, eds., American Society for Testing and Materials, 1998, pp. 114-134.
[87] Johnston, W. M., "Fracture Tests on Thin-Sheet 2024-T3 Aluminum Alloy for Panels with and without Buckling," NASA/CR (in progress), 1999.
[88] Young, R. D.; Rouse, M.; Ambur, D. R.; and Starnes, J. H., "Residual Strength Pressure Tests and Nonlinear Analyses of Stringer- and Frame-Stiffened Aluminum Fuselage Panels with Longitudinal Cracks," The Second Joint NASA/FAA/DoD Conference on Aging Aircraft, C. E. Harris, ed., NASA CP-208982, 1999, pp. 408-426.
[89] Seshadri, B. R.; Newman, J. C., Jr.; Dawicke, D. S. and Young, R. D., "Fracture Analysis of the FAA/NASA Wide Stiffened Panels," The Second Joint NASA/FAA/DoD Conference on Aging Aircraft, C. E. Harris, ed., NASA CP-208982, 1999, pp. 513-524.

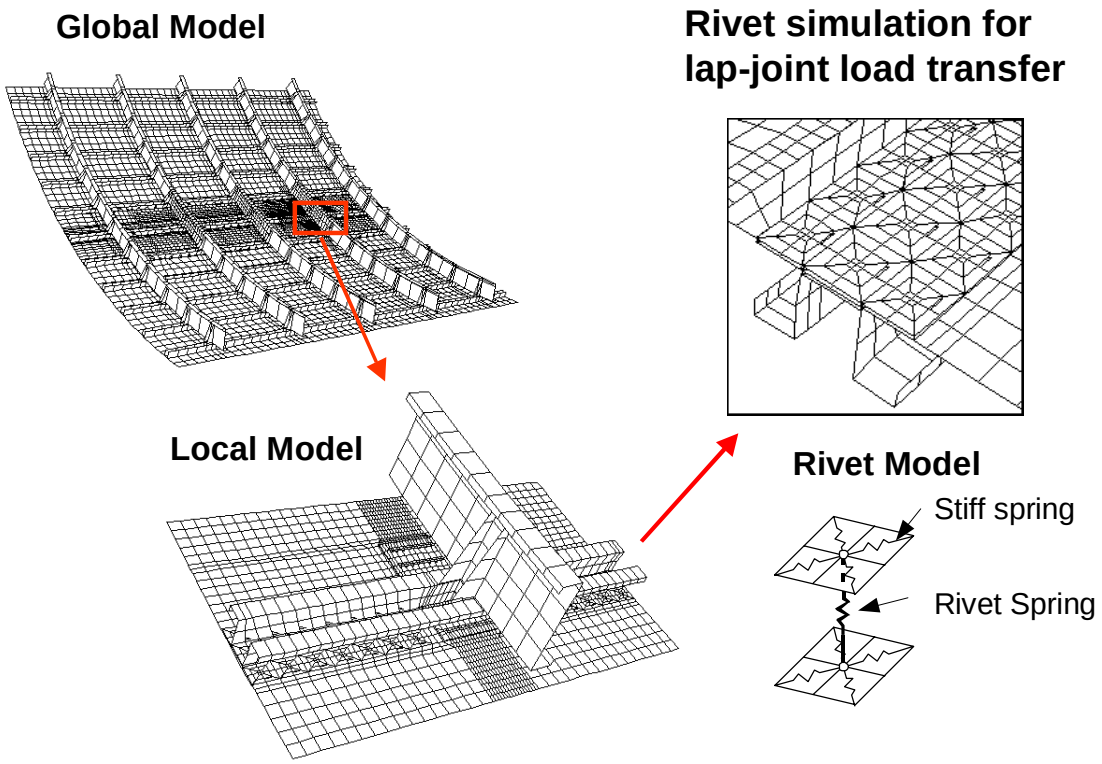

Figure 1. – Finite-element models from global to local stress analyses of fuselage structures.

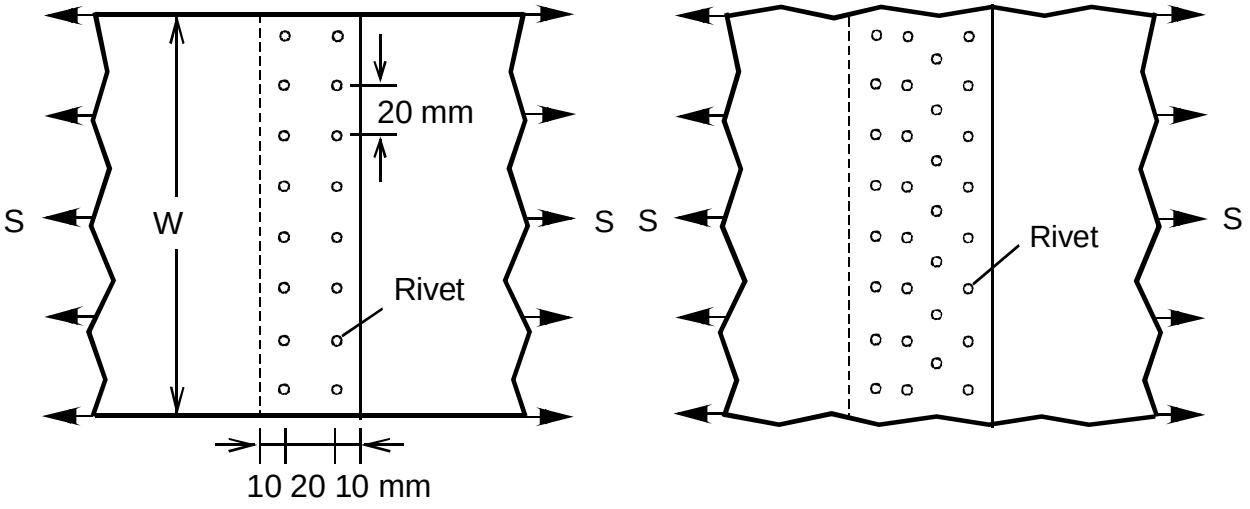

(a) NLR and KHI-NAL lap-joint specimens. (b) Full-scale fuselage test lap joint.

Figure 2. – Typical lap-splice joints specimens and joints in full-scale test article.

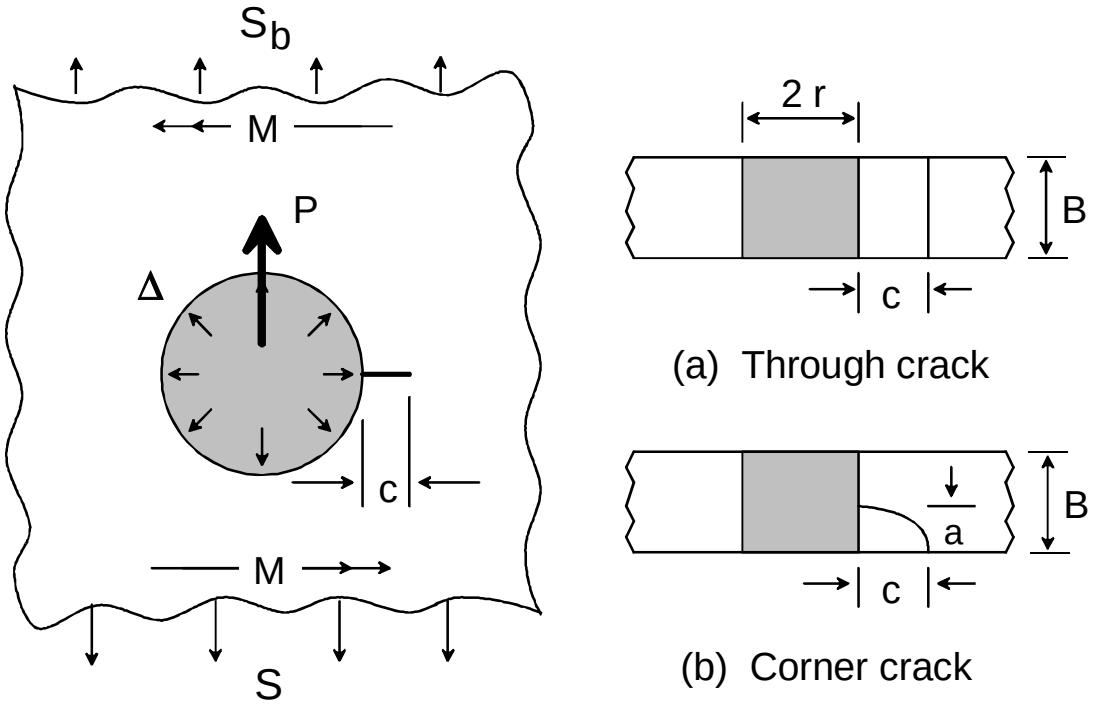

Figure 3. – Crack configuration and loading for rivet-loaded hole.

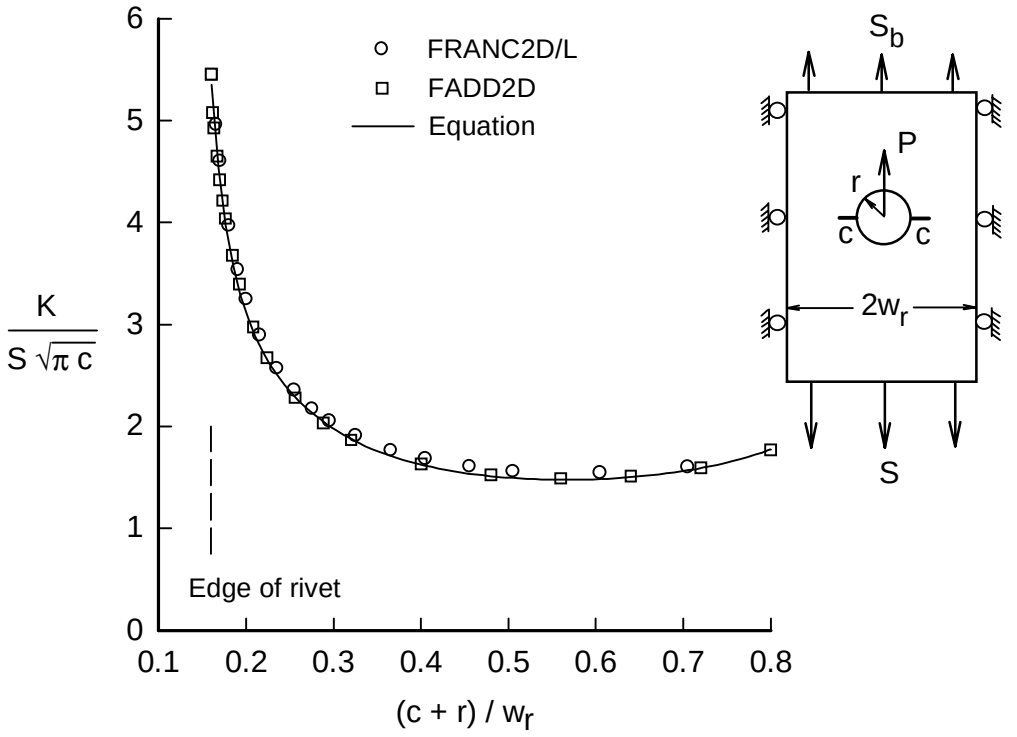

Figure 4. – Stress-intensity factors for through crack at rivet-loaded hole.

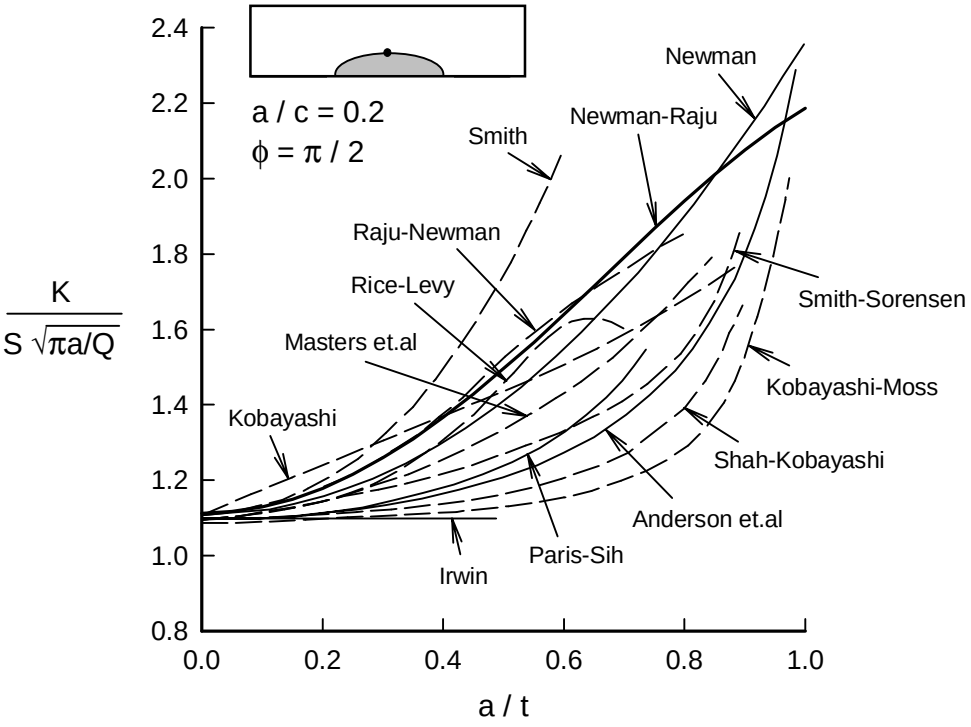

Figure 5(a). – Comparison of stress-intensity factors for semi-elliptical surface crack.

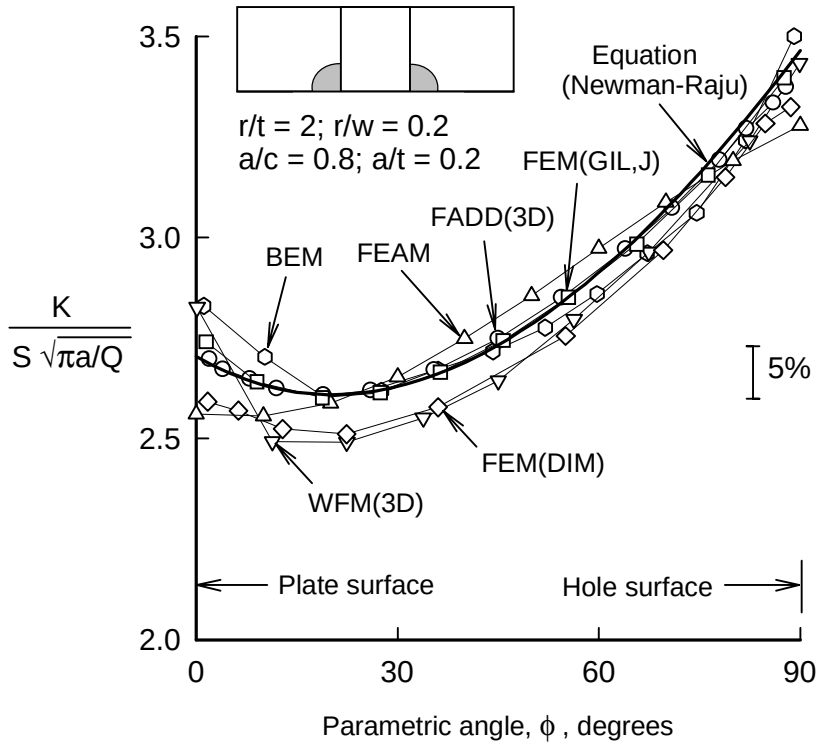

Figure 5(b). – Comparison of stress-intensity factors for quarter-elliptical corner crack at hole.

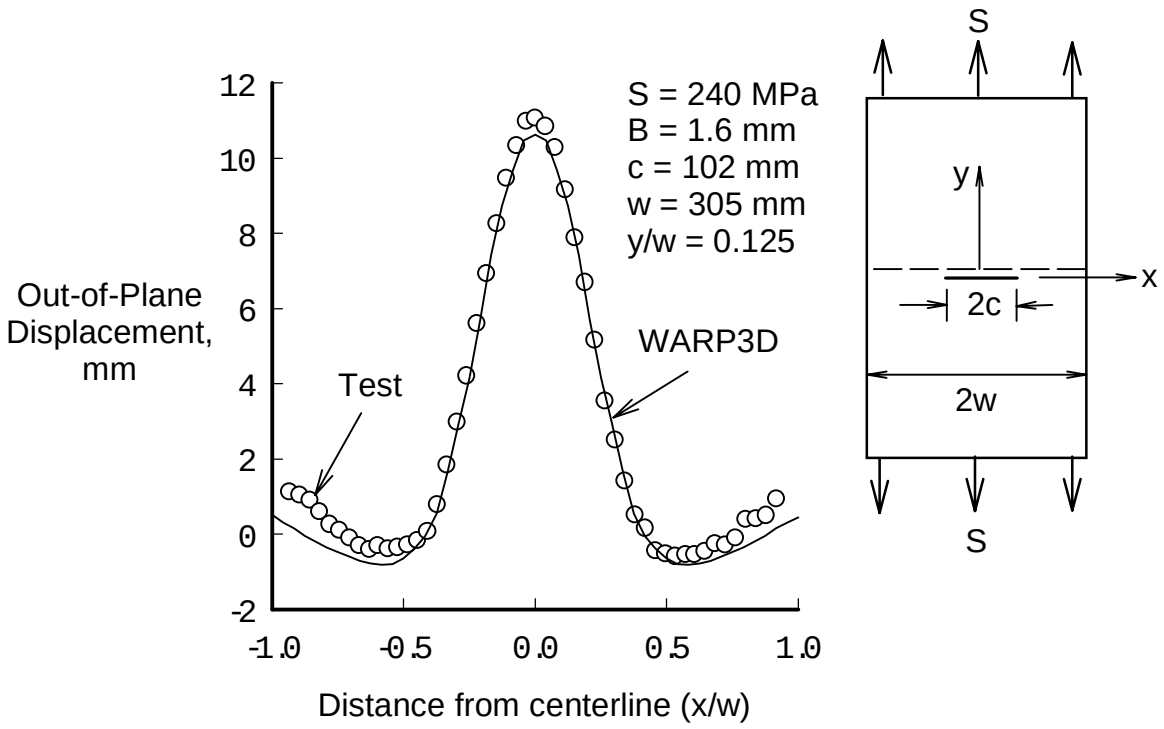

Figure 6. – Measured and calculated out-of-plane deformations in middle-crack tension specimen.

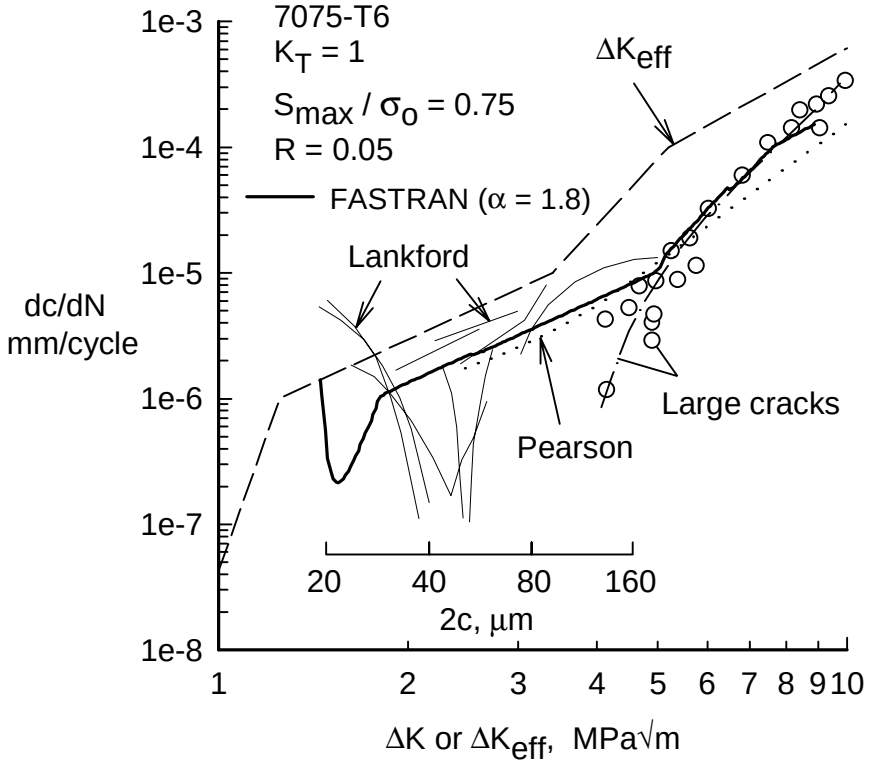

Figure 7. – Small- and large-crack data on 7075-T6 aluminum alloy from un-notched specimens.

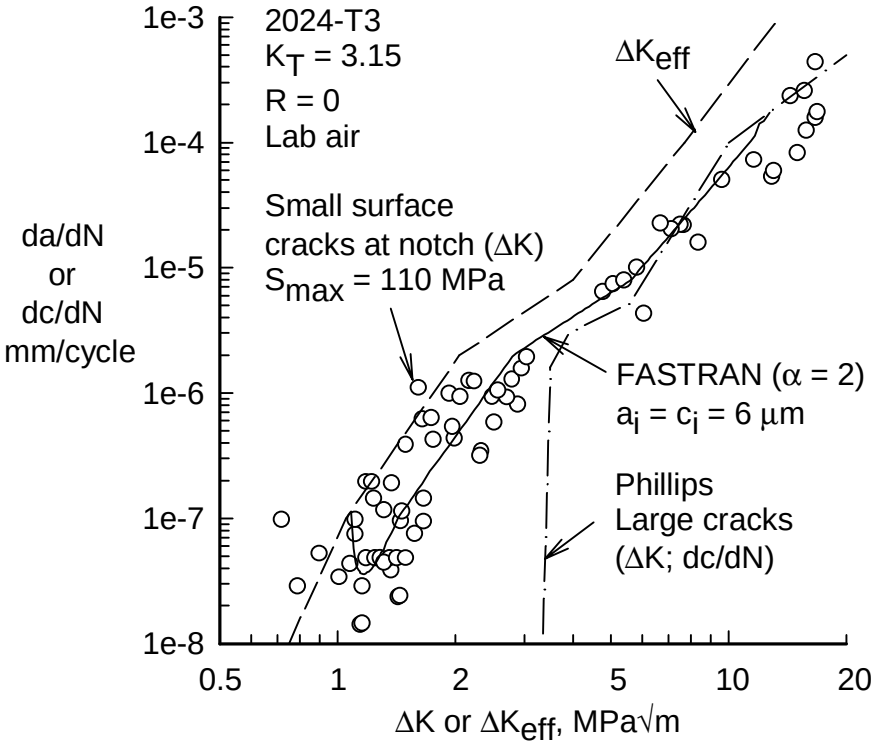

Figure 8. – Small- and large-crack data on 2024-T3 aluminum alloy from notched specimens.

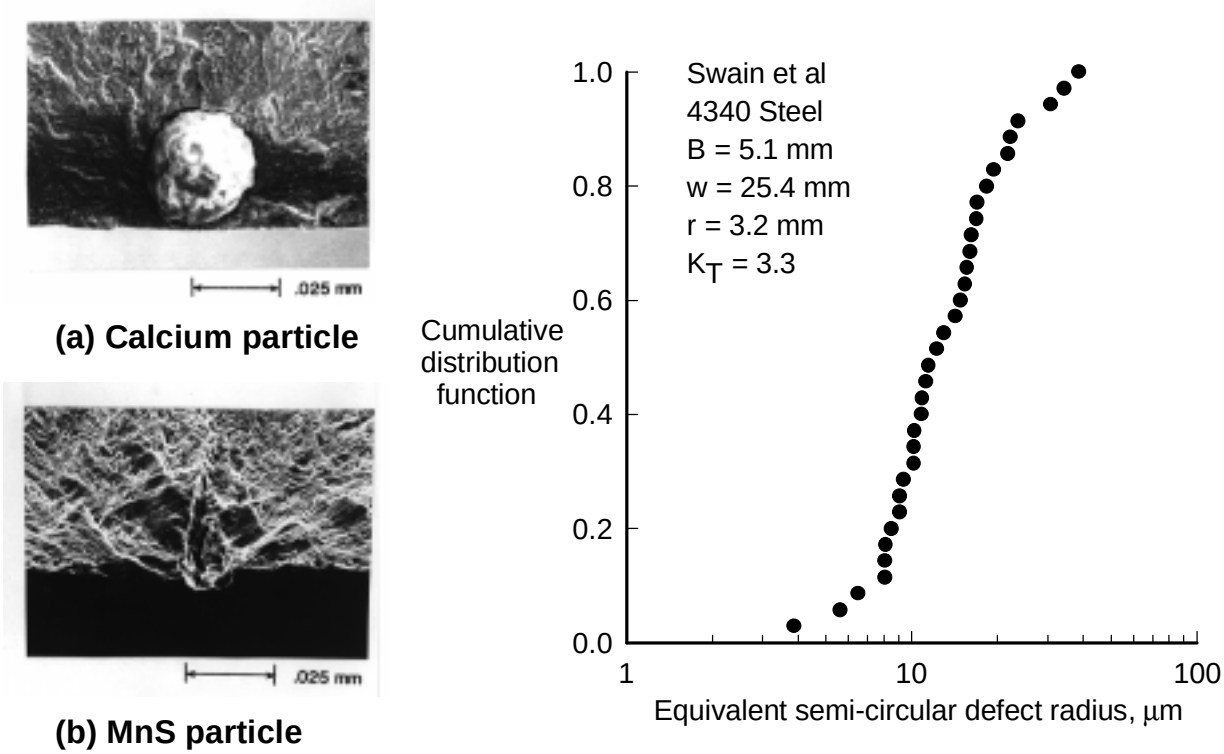

Figure 9. – Crack initiation sites and cumulative distribution function for 4340 steel.

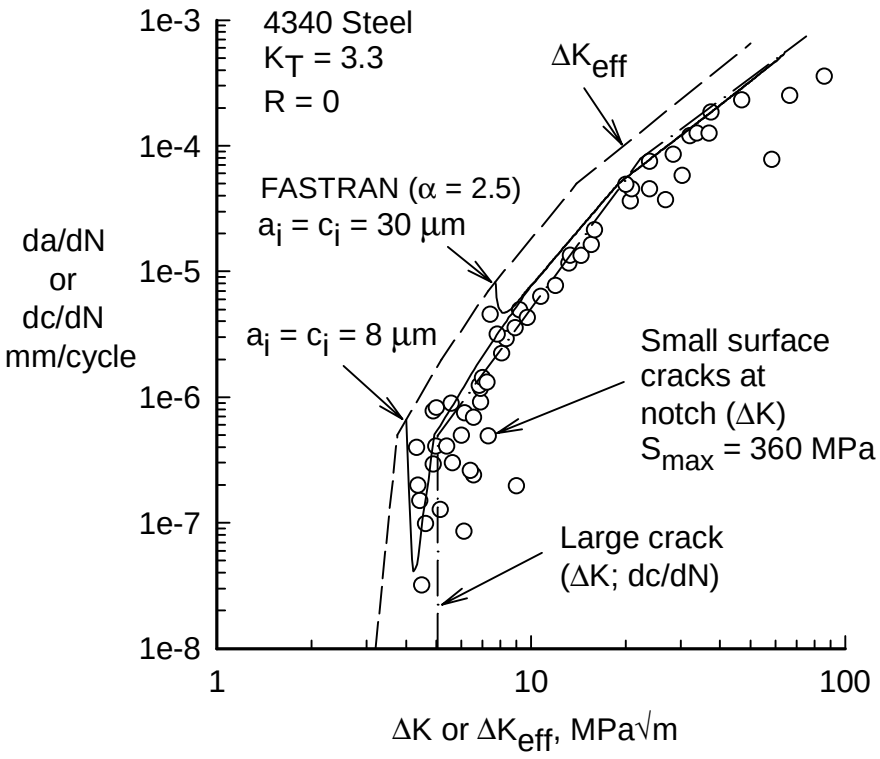

Figure 10. – Small- and large-crack data on 4340 steel from notched specimens.

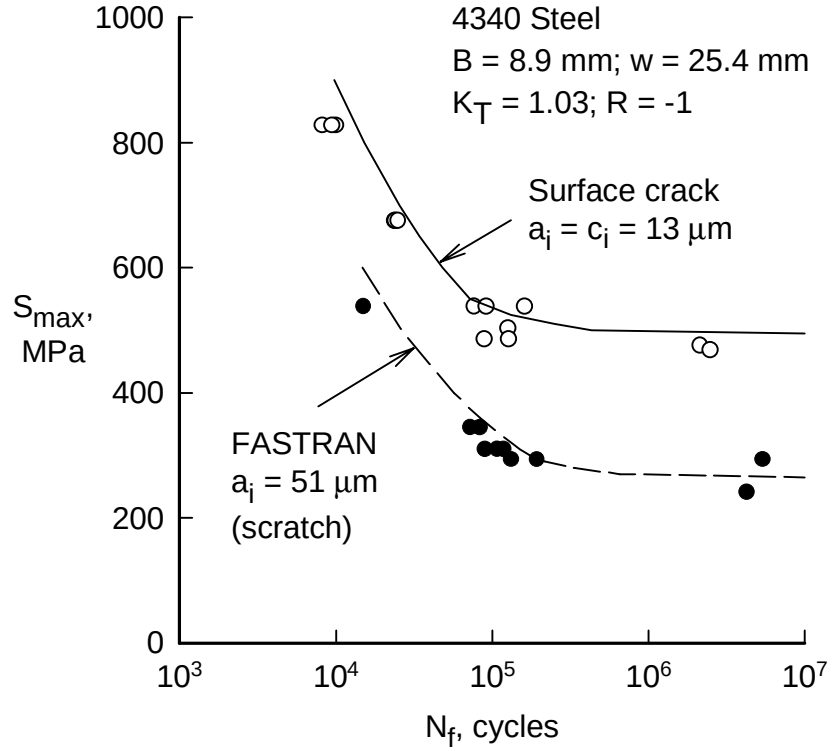

Figure 11. – Prediction of fatigue life on pristine and scratched specimens of 4340 steel.

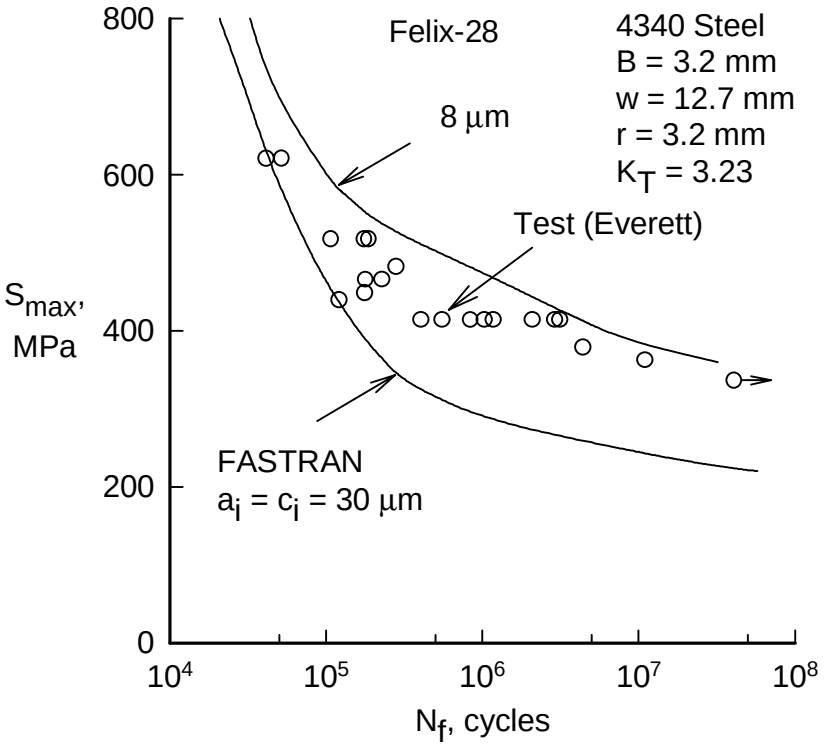

Figure 12. – Prediction of fatigue life on circular-hole specimens under Felix-28 spectrum.

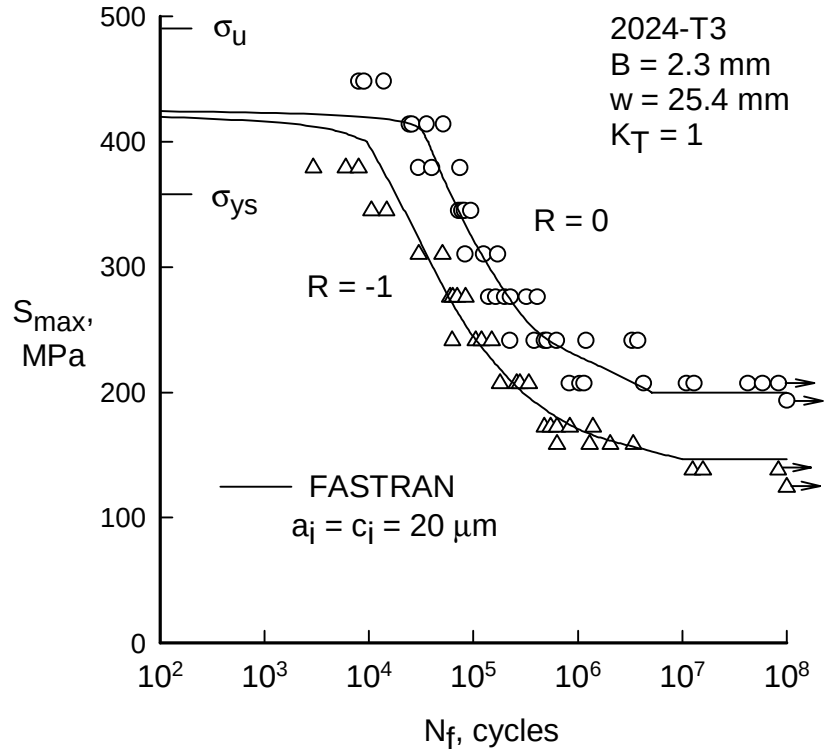

Figure 13. – Prediction of fatigue life on 2024-T3 for un-notched specimens at two stress ratios.

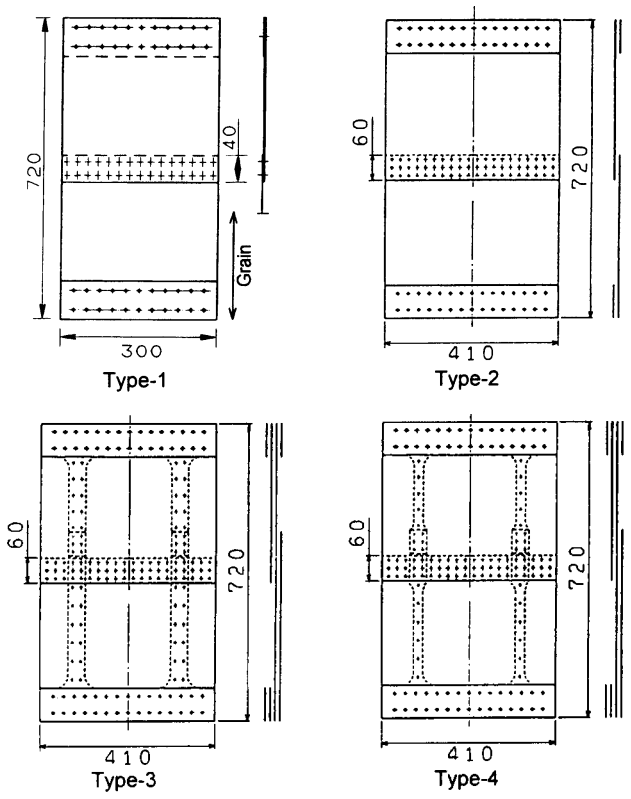

Figure 14. – Riveted lap-joint panels tested by Furuta, Terada and Sashikuma [24].

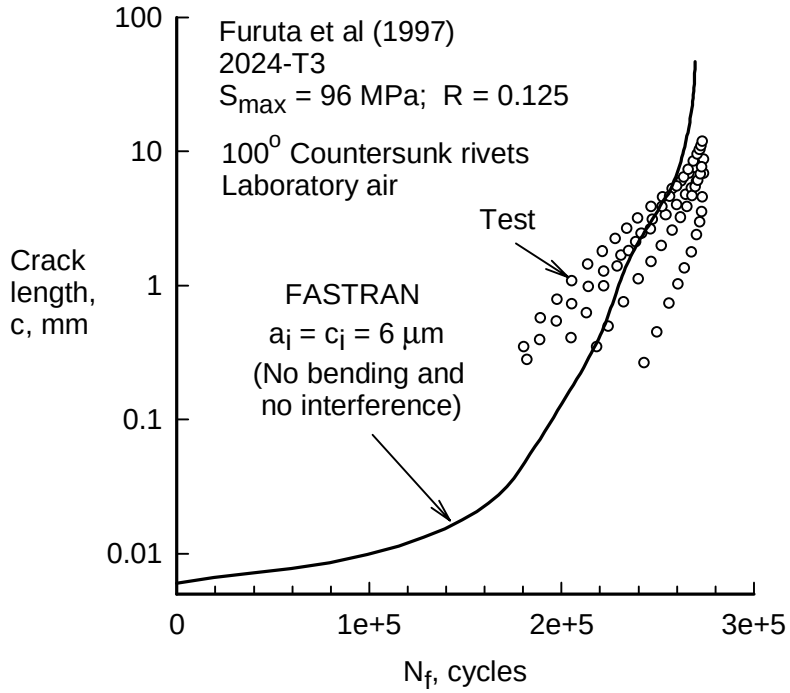

Figure 15. – Measured and calculated crack length against cycles for Type 1 lap joint under ambient conditions.

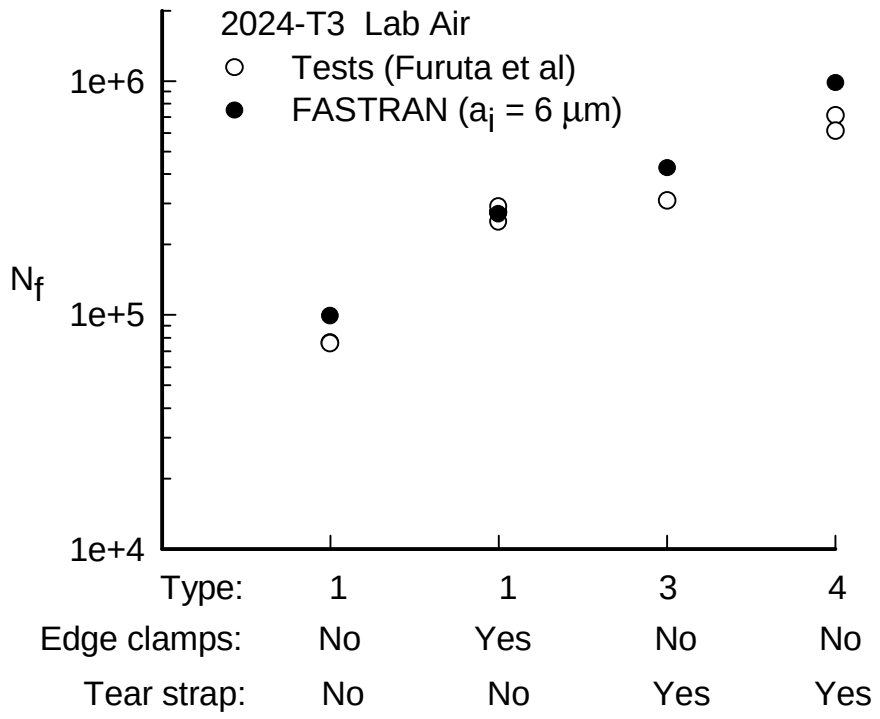

Figure 16. – Comparison of measured and calculated fatigue lives for various lap joints under ambient conditions.

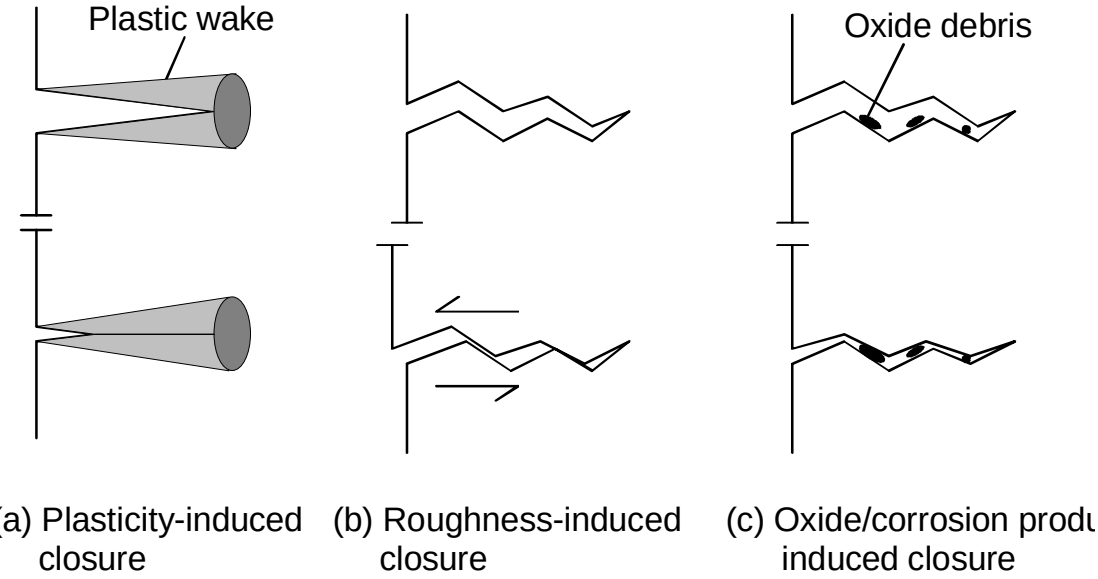

Figure 17. – Various forms of fatigue-crack-closure mechanisms.

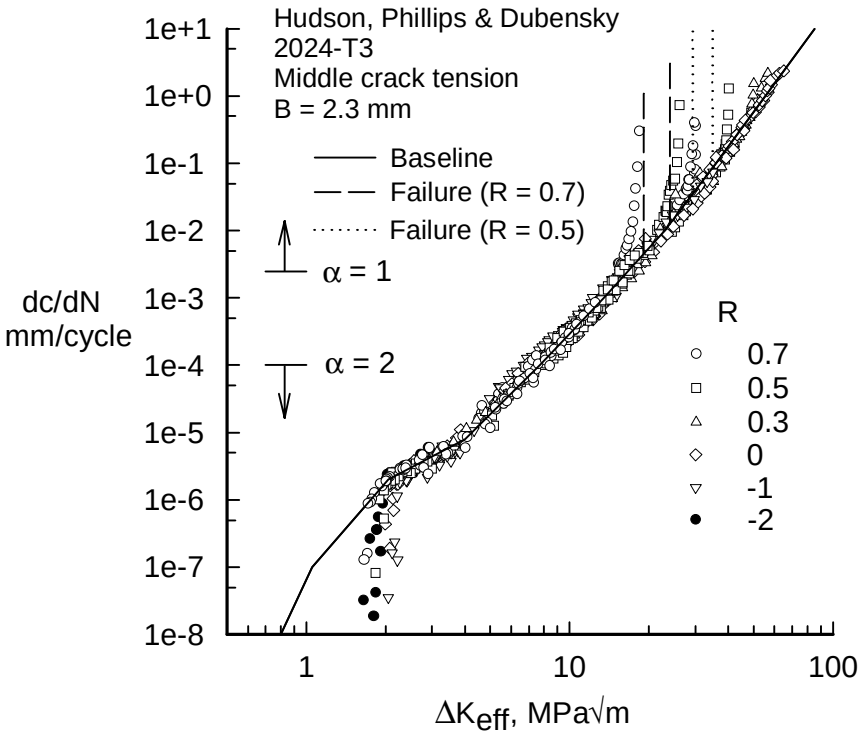

Figure 18. – Effective stress-intensity factor against crack-growth rate for 2024-T3 aluminum alloy over wide range in rates and applied stress levels.

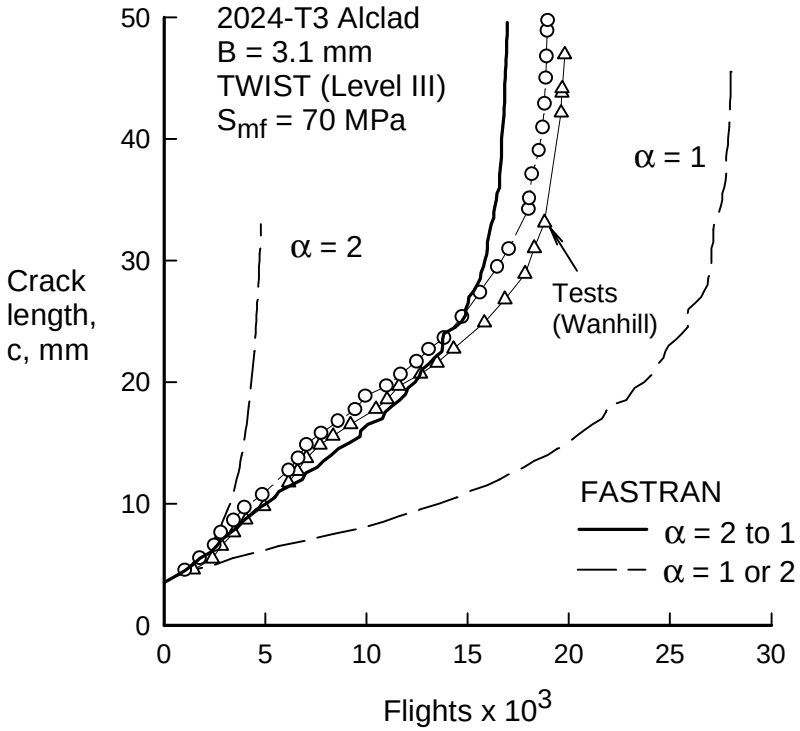

Figure 19. – Measured and predicted crack length against flights for thin-sheet 2024-T3 alloy under TWIST (Level III) loading.

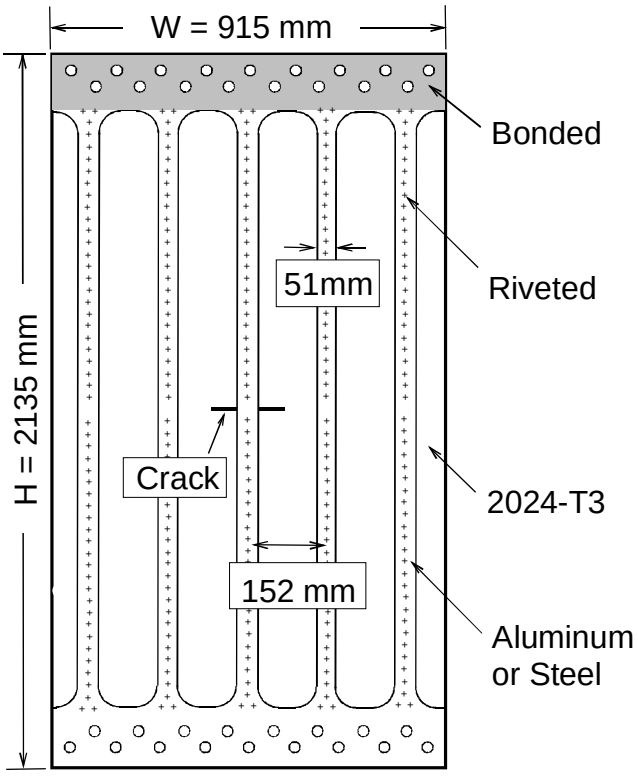

Figure 20. – Stiffened panel tested by Poe [71] to determine fatigue-crack-growth rates.

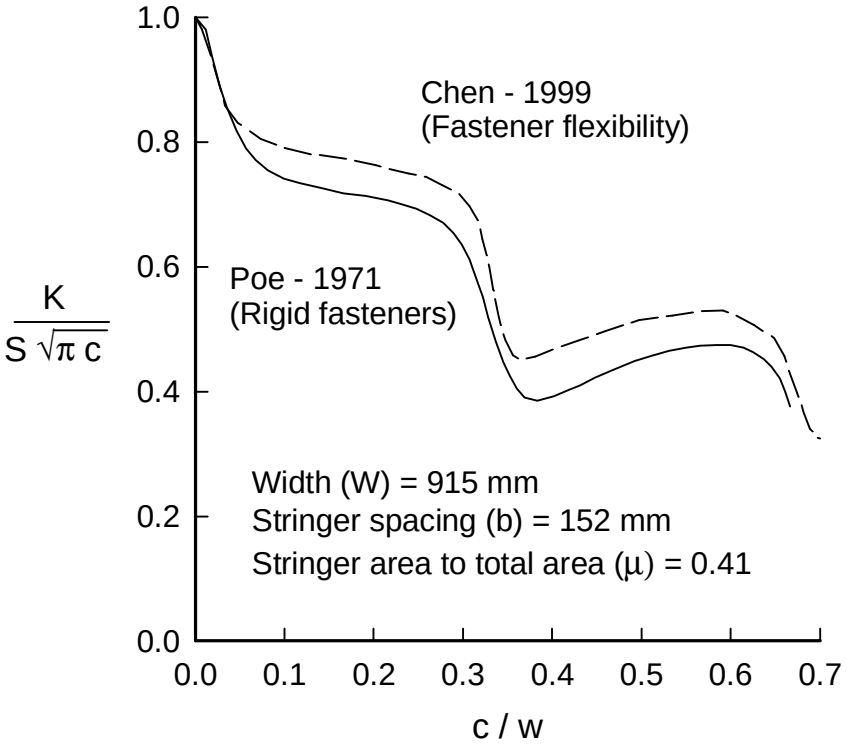

Figure 21. – Stress-intensity factors for cracked stiffened panel with rigid and flexible rivets.

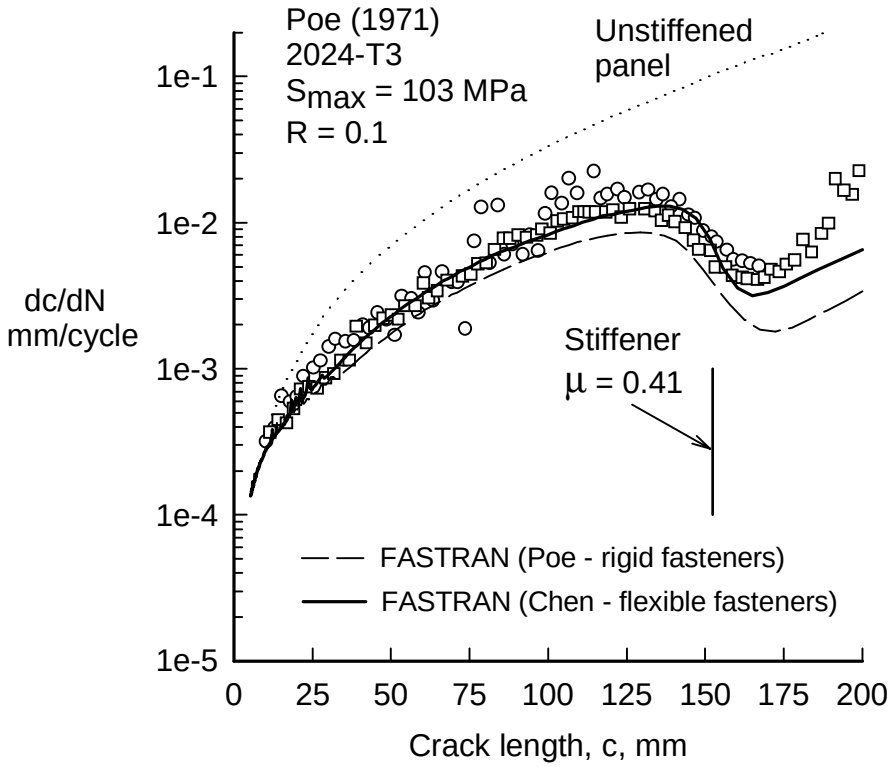

Figure 22. – Measured and predicted crack-growth rates for Poe's stiffened panel.

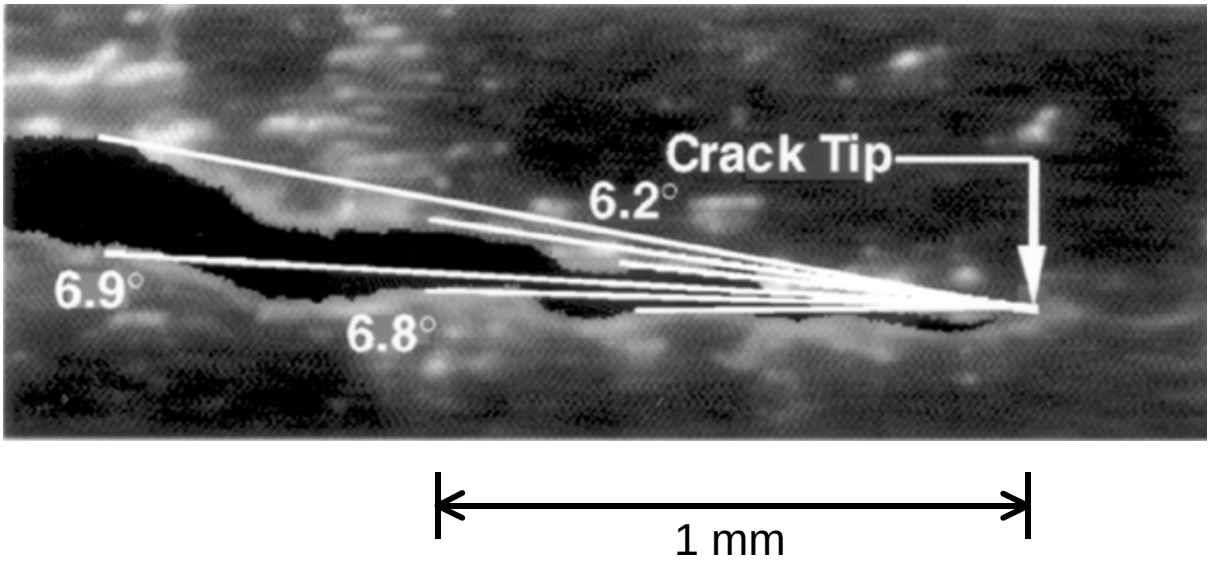

Figure 23. – Photograph of tearing crack and measurement of critical crack-tip-opening angle (CTOA).

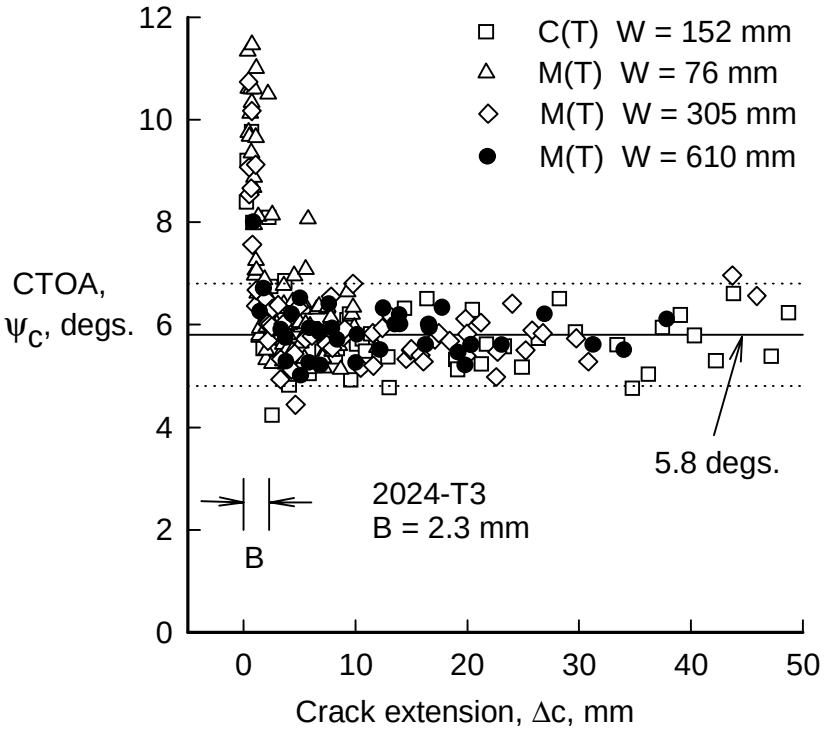

Figure 24. – Measurement of critical CTOA on compact and middle-crack tension specimens.

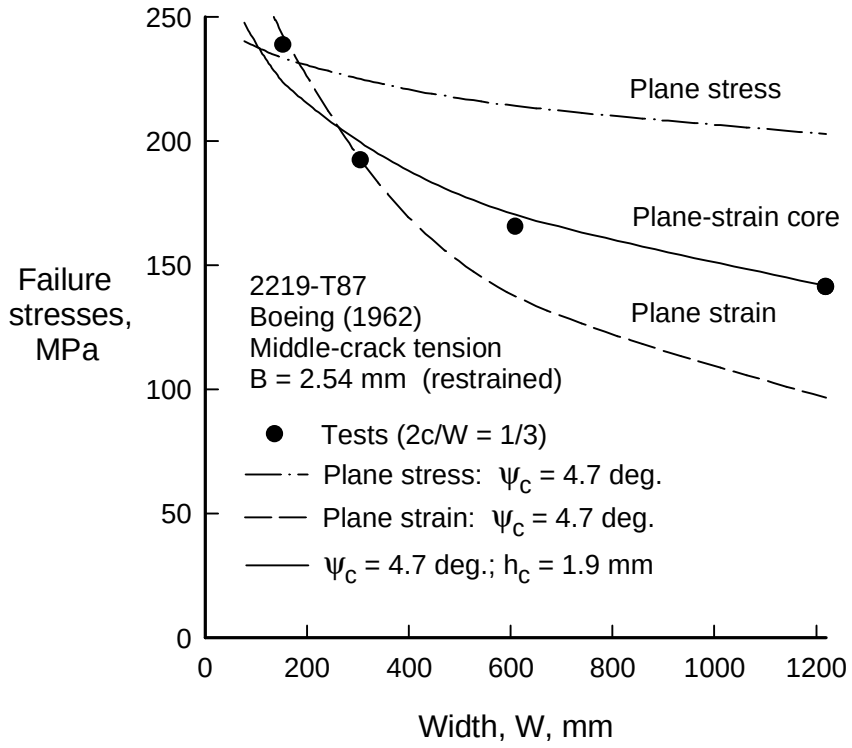

Figure 25. – Measured and calculated failure stresses on middle-crack tension specimens as a function of specimen width.

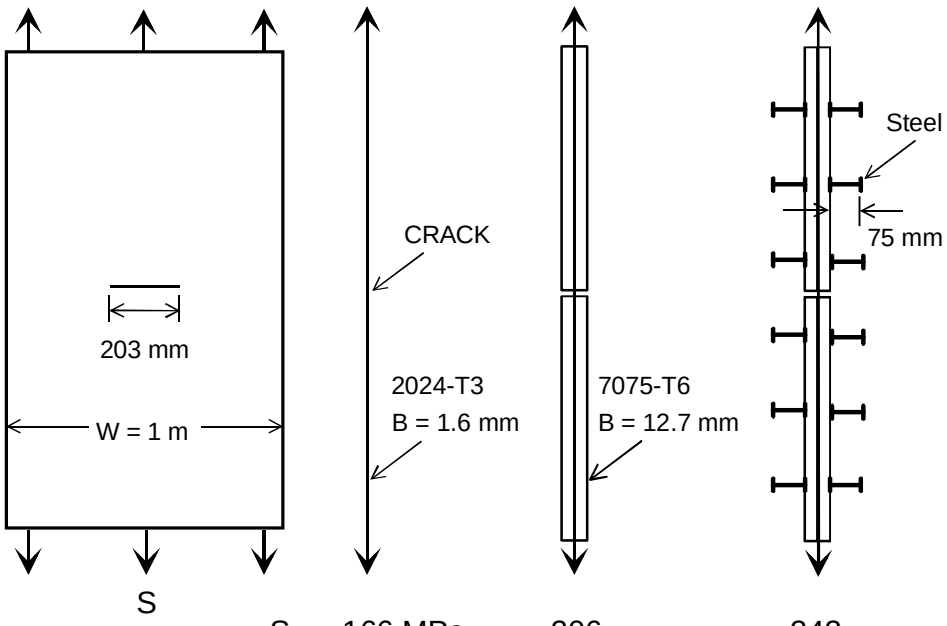

Figure 26. – Two anti-buckling guide plate systems to restrain middle-crack tension specimens.

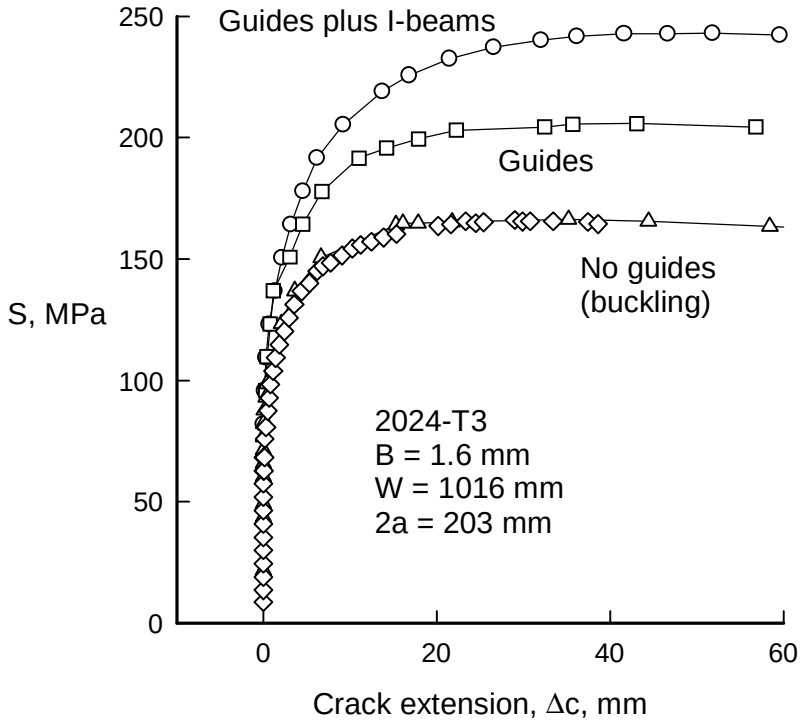

Figure 27. – Stable crack extension on wide middle-crack tension specimens with various anit-buckling guide systems.

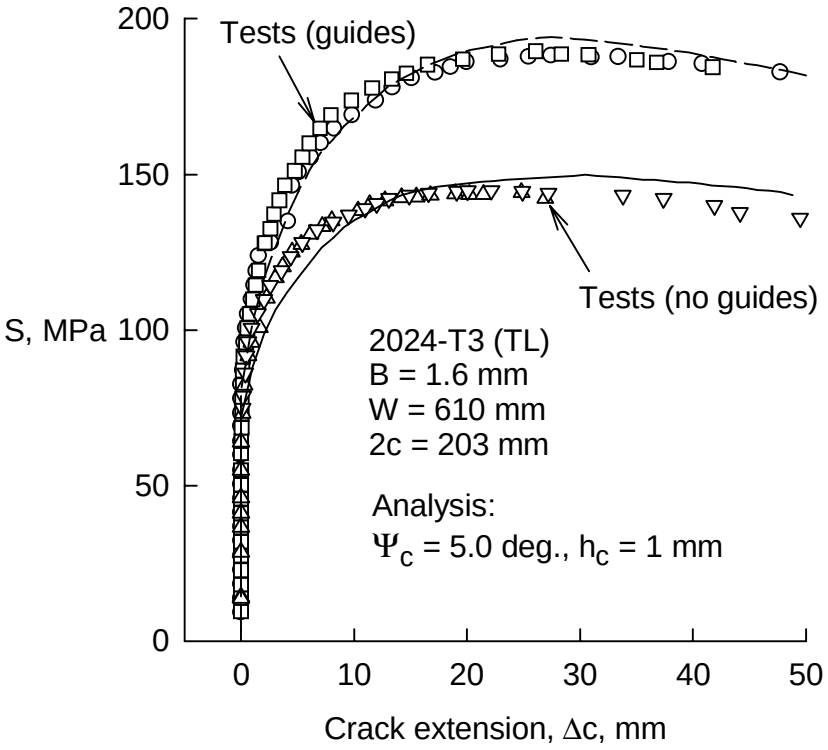

Figure 28. – Measured and predicted stable tearing under restrained and buckling conditions.

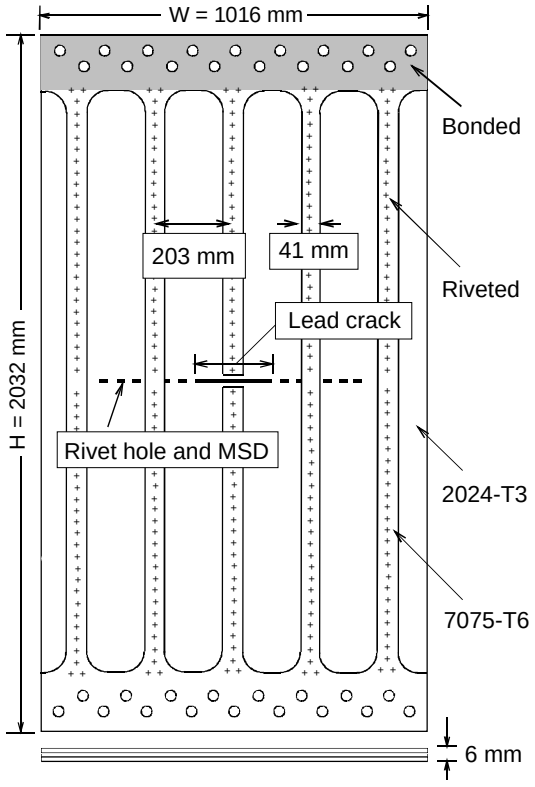

Figure 29. – FAA/NASA wide stiffened panel crack configuration.

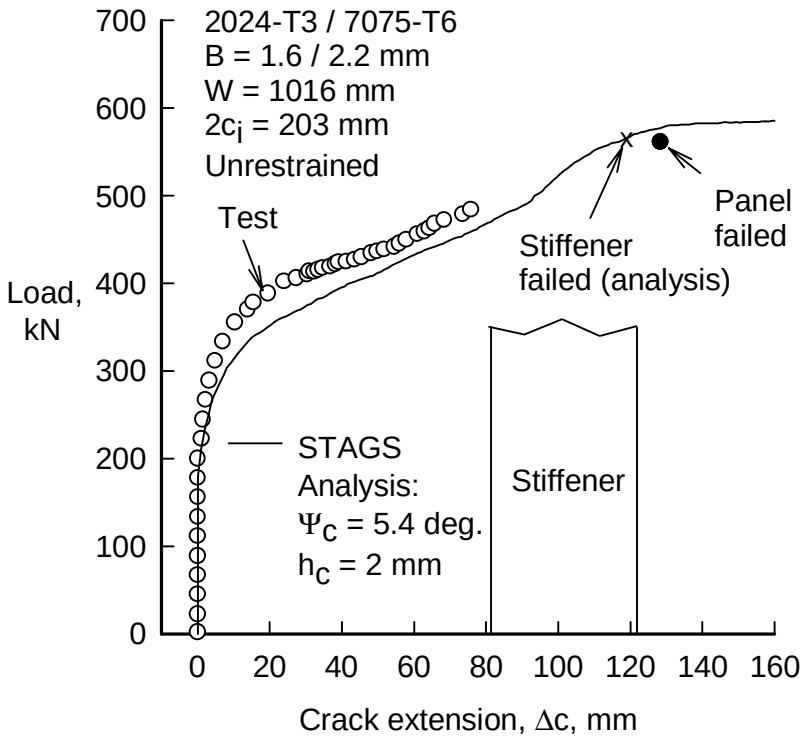

Figure 30(a). – Measured and predicted stable tearing in wide stiffened panel with a single crack.

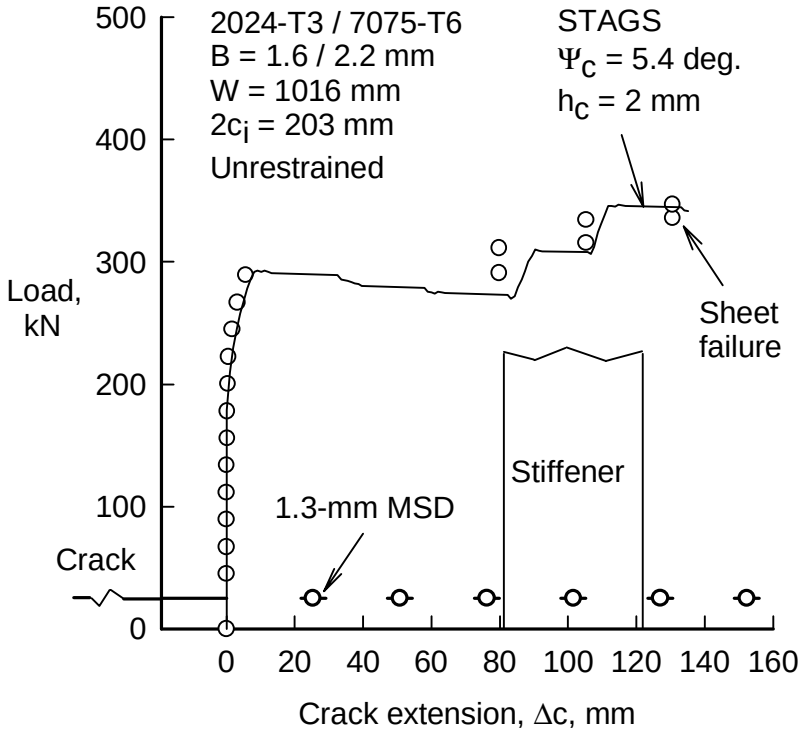

Figure 30(b). – Measured and predicted stable tearing in wide stiffened panel with a single crack and multiple-site damage cracking.